National Chiao Tung University

Department of Electrophysics

Thesis

鉍鐵氧-鈷鐵氧磊晶奈米複合薄膜之多鐵特性研究

Multiferroic Properties of BiFeO$_3$-CoFe$_2$O$_4$ Epitaxial Nanocomposite

Thin Film

Student: TahtaAmrillah
Advisor: Prof. Jenh-YihJuang

August, 2014

鉍鐵氧-鈷鐵氧磊晶奈米複合薄膜之多鐵特性研究

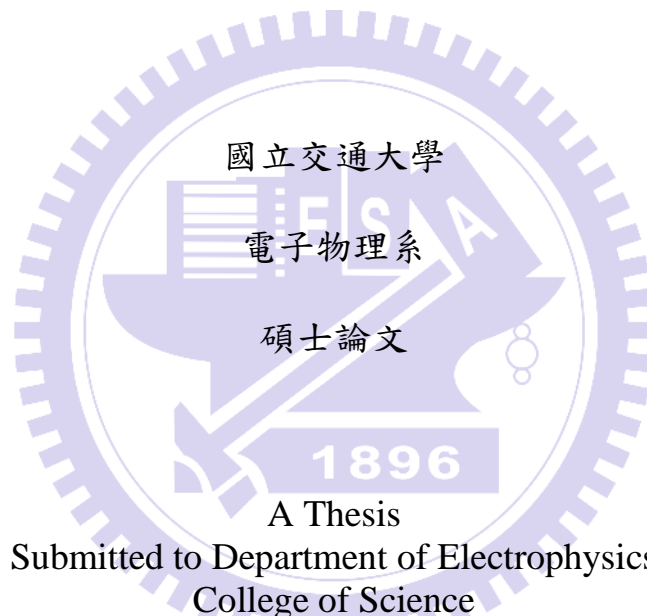## Multiferroic Properties of BiFeO$_3$-CoFe$_2$O$_4$ Epitaxial Nanocomposite Thin Film

研究生: 安泰達 Amrillah

Student: Tahta Amrillah

指導教授: 莊振益

Advisor: Jenh-Yih Juang

國立交通大學

電子物理系

碩士論文

A Thesis
Submitted to Department of Electrophysics
College of Science
National Chiao Tung University
in partial Fulfillment of the Requirements
for the Degree of
Master of Science
in

Electropysics

August 2014

Hsinchu, Taiwan, Republic of China

中華民國一百零三年八月

鉍鐵氧-鈷鐵氧磊晶奈米複合薄膜之多鐵特性研究

研究生：安泰達　　　　　　　　　　　指導教授：莊振益

國立交通大學

電子物理系

中文摘要

當利用雷射蒸鍍技術成長鉍鐵氧(BFO)與鈷鐵氧(CFO)薄膜於鈦酸(STO)基板時，透過改變其鍍膜條件，可以成功製備出垂直排列之 BFO-CFO 奈米複合結構。從 X 射線繞射分析儀可以得知，STO 基板會對 BFO 與 CFO 薄膜造成應變效應。特別是在 BFO-CFO/STO 的垂直排列奈米複合結構(VAN)中，CFO 晶柱將使得 STO 基板對 BFO 造成之應變效應產生垂直方向上的應力鬆弛，進而讓磁相變溫度產生位移，其中 BFO 粉末的磁相變溫度約在 55K 與 200K；BFO/STO 薄膜的磁相變溫度則在 30K 與 160K 附近。而從 BFO/CFO/STO 雙層薄膜及 BFO-CFO/STO VAN 的 M-T 與 C-T 量測中我們可以得知，反鐵磁-鐵磁(BFO-CFO)的耦合強度較反鐵磁-鐵電(BFO)的耦合強度為強，使得此系統之其磁化強度及電容的相變不易被觀察到。此外，

BFO/STO 與 BFO/CFO/STO 的 C-T 特性十分相似，兩者間僅有細微的差異，推測為淬火時 BFO 與 CFO 的鐵磁耦合使得電子在 BFO 中發生自旋的重新取向導致，這個現象在 CFO 晶柱埋於 BFO 環境中時則更為複雜。最後，從 R-T 量測中，高密度的 BFO-CFO/STO VAN 薄膜在 30K 附近表現出了明顯的絕緣體-金屬轉變，而這個溫度也低於其他研究者在外加強力磁場下所觀察到 BFO 薄膜的轉變溫度。由此結果我們推測，當晶柱密度足夠大時，將有可能產生一個足夠大的局部磁場，並藉此調變 BFO 環境中的電域結構。更深入的介紹與探討將會在本文中呈現。

Multiferroic Properties of $BiFeO_3$-$CoFe_2O_4$ Epitaxial Nanocomposite Thin Film

Student: Tahta Amrillah   Advisor: Prof. Jenh-Yih Juang

Department of Electrophysics

National Chiao Tung University

ABSTRACT

BFO-CFO vertically align nanocomposite (VAN) was successfully made by utilizing the different wetting conditions from BFO and CFO film when growing on STO substrate at the same time in the PLD system. From the XRD result, there was strain effect from STO substrate to BFO and CFO film. Especially for BFO-CFO/STO VAN, CFO pillar relaxed the strain of BFO film, and shifted magnetic phase transitions on BFO/STO thin film to around 30 K and 160 K as compared to that of BFO powders where the transitions occured around 55 K and 200 K, respectively. From M-T and C-T measurements on BFO/CFO/STO bilayer and BFO-CFO/STO VAN, antiferromagnetic-ferromagnetic coupling (BFO-CFO) is stronger than antiferromagnetic-ferroelectric coupling (BFO). making the magnetization and capacitance anomalies unobservable in those

systems. Furthermore, the C-T beharviors of BFO/STO and BFO/CFO/STO are in general similar, but different in subtle details, which presumably originates from the quenching of spin reorientation in BFO due to ferromagnetic coupling from CFO. The situation is even more complicated in the CFO pillar embedded in BFO matrix sample. Finally, from R-T measurement, the high-density BFO-CFO/STO VAN film showed an apparent insulator-metal transition around 30 K, which is similar to that observed in BFO film under strong external magnetic fields which done by another reseach before. The result suggests that when the pillar density is large enough it may generate strong enough local magnetic field to modify the ferroelectric domain structures in BFO matrix. Further investigations are certainly in order to delineate the interisting emergent phenomena observed in the present study.
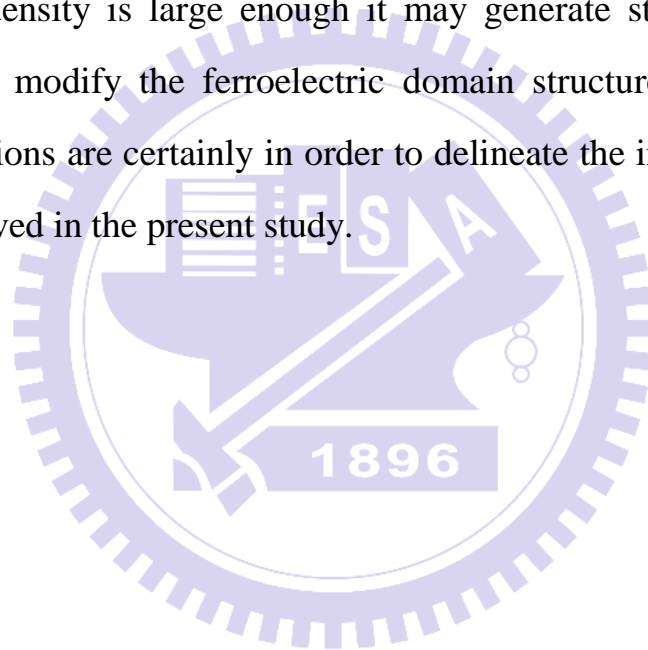
Acknowledgement

First I want to thank to my Lord, ALLAH S.W.T with His affection and opportunity for my life, I could do anyting, especially to do this reseach. I take this opportunity to express my profound gratitude and deep regards to my Advisor, Prof. Jenh-Yih Juang for his exemplary guidance, monitoring and constant encouragement throughout the course of this thesis. The blessing, help and guidance given by him time to time shall carry me a long way in the journey of life on which I am about to embark.

I also take this opportunity to express a deep sense of gratitude to all my colleagues and labmates, for their support, valuable information and guidance, which helped me in completing this task through various stages.
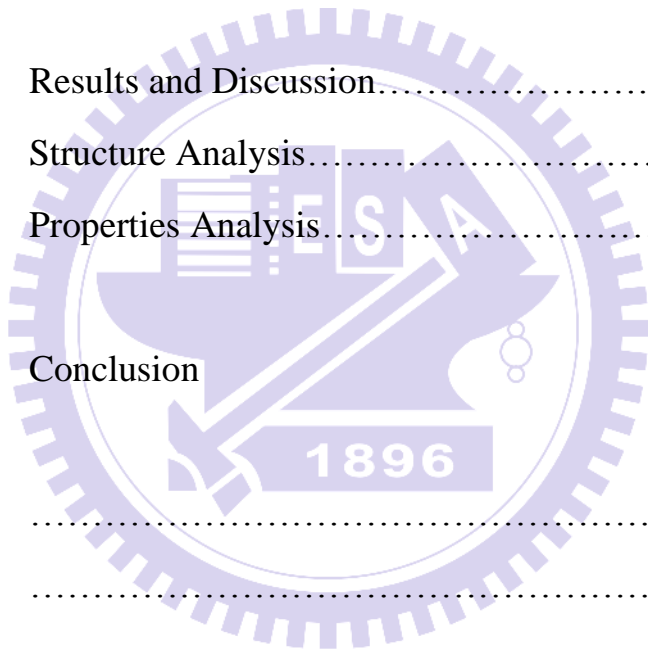
Lastly, I thank almighty, to my wife who gave me support all the time, my parents, brother, sisters and friends for their constant encouragement without which this assignment would not be possible.

Contents

List of Table

List of Figure

I. Introduction

Recently, memory and sensor devices based on the spintronic technology have been of extensive reseach. One of the main streams in this reseach area is to manipulate the material system exhibiting the desirable magneto-electric properties with the aids of advanced nanotechnologies. Among the numerous magnetic materials being investigated worldwide, $BiFeO_3$ (BFO) has received perhaps the most attention over the last decade. BFO is a multiferroic material simultaneous possesing magnetic and ferroelectric orders at room temperature [1], which allows one to manipulate the two order parameters and gives rise to rich unprecedented emergent physical properties.

In addition to being more appropriate for various device applications, thin film BFO has been demonstrated to exhibit superior physical properties over its powder and/or bulk counterpart, as well [1]. For instance, BFO has been succesfully grown on various kinds of substrates, such as $SrTiO_3$ and Pt/Ti/SiO/Si, by various processing methods, such as pulse laser deposition (PLD), sputtering, molecular beam epitaxy (MBE), as well as chemical vapor deposition (CVD). Consequently, many interesting intrinsic properties of BFO have been thoroughly explored in the literature.

Nevertheless, in order to further manipulate and improve the functionalities of BFO-based devices, proposals of combining BFO thin film with other magnetic material are receiving more and more reseach attention. In the present study, we are aiming at combining another magnetic material $CoFe_2O_4$ (CFO) with BFO to explore the emergent properties that might arise in this composite system. Since CFO is a ferromagnetic material, it is expected that, by properly designing the composite in nanoscale through careful substrate selection and deposition process, ferromagnetic coupling and magnetostriction imposed by CFO may further modify the properties of BFO. Hence, new functionalities might be obtained. For example, as depicted schematically in Fig. 1.
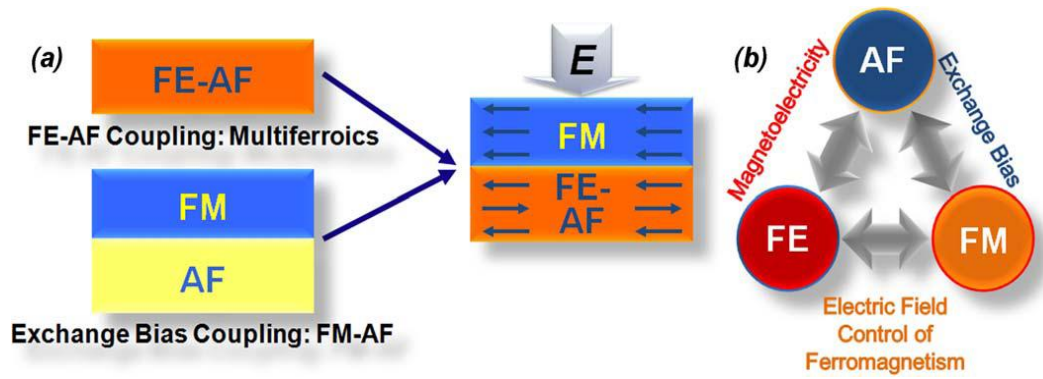
Figure 1. Possible properties that might occur by combining of BFO (multiferroic) and CFO (ferromagnetic) [1].

Due to the antiferromagnetic-ferromagnetic coupling between BFO and CFO. One might be able to realize the controlled ferroelectricity or vice versa. In this reseach we tried to fabricate different combinations of these two interesting materials and investigate the associated magnetic and electric properties down to low temperatures.

II. General Backgrounds

2.1 Structureof $BiFeO_3$, $CoFe_2O_4$, $SrTiO_3$ and Self Assembly Epitaxial Thin Film by PLD

The modern study of complex oxide materials has been driven largely by the development of new growth and characterization techniques that have offered researchers unprecedented access to new phases and insight about these materials [2]. Epitaxial growth of thin films offers a pathway to the discovery and stabilization of a number of new multiferroics in conjunction with the availability of high quality materials that can be produced with larger lateral sizes than traditionally possible with single crystal samples [1].

By selecting materials that spontaneously separate due to immiscibility, such as spinel and perovskite phases [3], one can create nanostructured phases made of pillars of one material embedded in the matrix of another. The large difference in lattice parameter between these phases leads to the formation of pillars with dimensions on the order of tens of nanometers, which ensures a high interface-to-volume ratio, an important parameter when attempting to couple the two materials via strain. These nanostructures, in which the interface is perpendicular to the substrate, remove the effect of substrate clamping and allow for better strain-induced coupling between the two phases. An explosion of research into alternate material systems followed as the design algorithm proved to be widely applicable to many perovskite-spinel systems [1]. In this reseach we tried to extend such concept by combining BFO (perovskite) - CFO (spinel) materials together on STO substrate to form nanoscale composite thin film by PLD.

$BiFeO_3$ is a popular multiferroic that displays both ferroelectric and antiferromagnetic behaviors at room temperature. Bulk $BiFeO_3$ at room temperature possesses rhombohedral symmetry, space group $R3c$ (point group

3

$3m$), with lattice constants a=5.5785 Å and c=13.8688 Å [1]. Figure 2 shows the pictorial illustratlion of the prominent features of the crystal structure, ferroelectric polarization, and magnetic structures of $BiFeO_3$. But Unfortunately, $BiFeO_3$ is very unstable at the high temperature of the β–γ transition and it rapidly decomposes into parasitic phases such as $Bi_2Fe_4O_9$ or Fe_2O_3 [4].
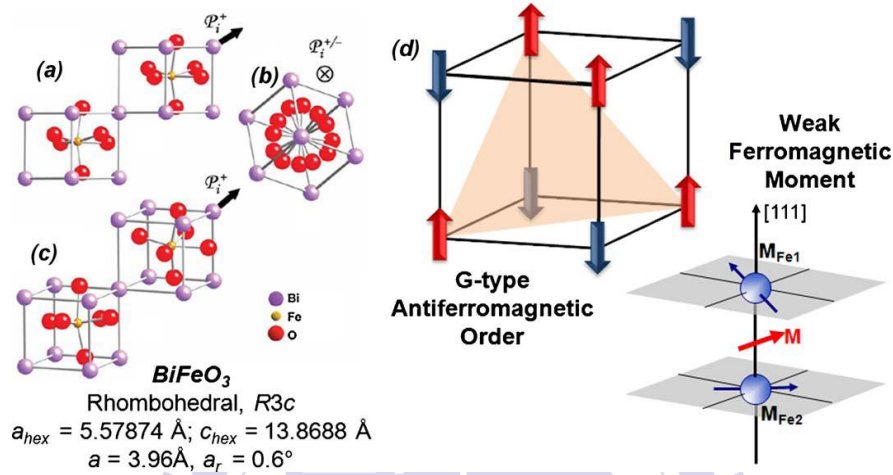
Figure 2. Structure of $BiFeO_3$ shown looking (a) down the pseudocubic-[1 1 0], (b) down the pseudocubic-[1 1 1] polarization direction, and (c) a general three dimensional view of the structure, (d) The magnetic structure of $BiFeO_3$ is shown including G-type antiferromagnetic ordering and the formation of the weak ferromagnetic moment [1].

$BiFeO_3$ (BFO), have attracted a lot of attention with respect to potential application in ultrahigh density memory devices [5]. In thin films, $BiFeO_3$ possesses a spontaneous electric polarization (P_s) of ~100 μC/cm^2, the highest of any known ferroelectric materials. This is also an order of magnitude greater than that originally reported for bulk $BiFeO_3$ samples, which gave rise to a flurry of work exploring the film symmetry to elucidate any structure property relations [6].

$CoFe_2O_4$ belongs to the family of spinels. The spinel family is a group of compounds with a general formula of AB_2X_4 (A and B are cations; X is an anion, i.e. O, S, Se, Te). The spinel structure shown in figure 3 is named after

the mineral spinel, $MgFe_2O_4$, which is the parent compound in this group. There are eight formula units per cubic unit cell, each of which consists of 32 anions and 24 cations, for a total of 56 atoms. As a consequence, the spinel lattice parameters are large, for $CoFe_2O_4$ a = 8.38 Å. The 32 anions, i. e., O^{2-}, are arranged in a face-centered cubic (f.c.c) lattice. There are 64 tetrahedral interstices (A sites) that exist between the anions, 8 of them are occupied by cations. There are 32 octahedral interstices (B sites) between the anions, 16 cations occupy half of the sites [7, 8].
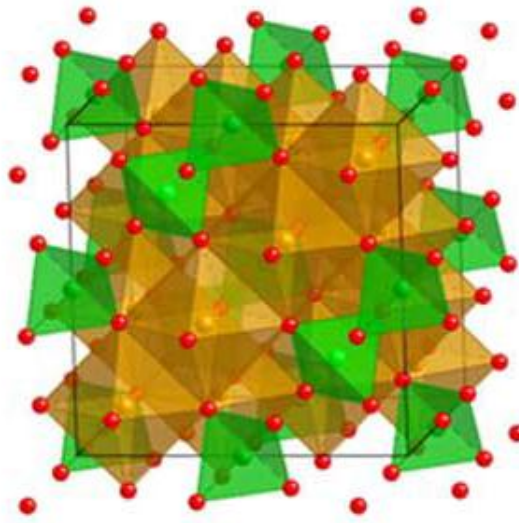
Figure 3. Crystal Structure of $CoFe_2O_4$ [1].

Strontium–titanate, $SrTiO_3$ (STO), falls within the class of perovskite-type oxides, The general formula for a perovskite is ABO_3 where A and B are cations. The A cations occupy every hole which is created by 8 BO_6 octahedra, giving the A cation a 12-fold oxygen coordination, and the B-cation a 6-fold oxygen coordination, as shown in Figure 4 [9]. STO is widely used on a large scale as substrate material for the growth of thin film perovskite type materials like BFO. Development of PLD process has enabled the realization of making, like growing BFO-CFO nanocomposite on STO substrate. Combination of different properties and different structures among them often leads to new observation of basic properties emerged in materials.
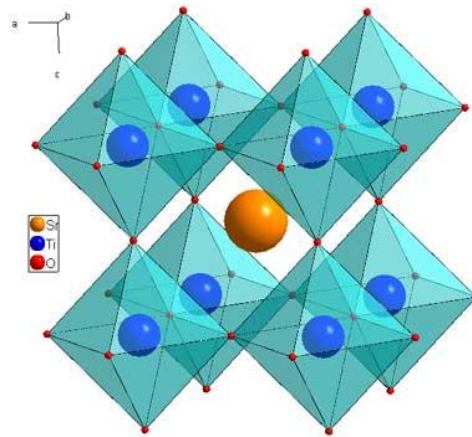
Figure 4. STO crystal structure [9].

In this study, we fabricate of BFO-CFO composite thin film with design structures such as multilayer and vertically aligned nanocomposite. The main difference of multilayer and vertically aligned nanocomposite design are realized by manipulating the nucleatiation and growth during PLD process. Namely, by controlling the growth condition, the film growth mode can be turned to proceed with the : Volmer–Weber (island growth), Frank–Van der Merwe (layer-by-layer growth), and Stranski–Krastanov growth.
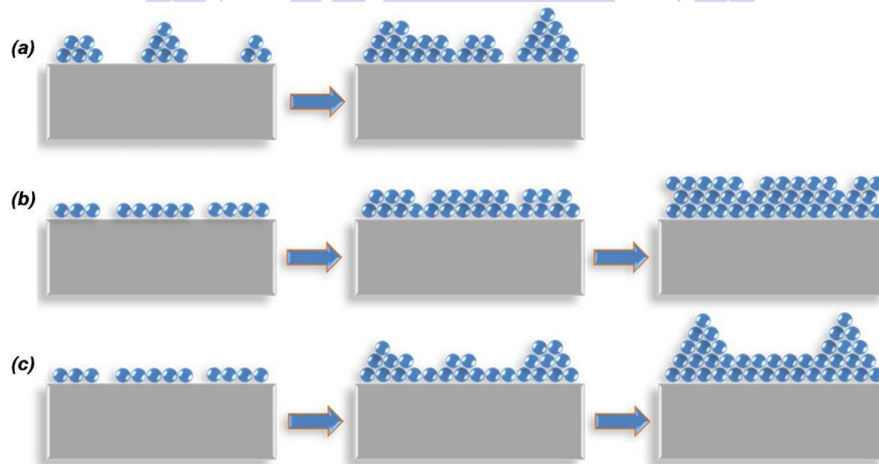
Figure 5. Typical growth modes (a) Volmer–Weber (island), (b) Frank–Van der Merwe (layer-by-layer), and (c) Stranski–Krastanov growth [1].

The Volmer–Weber (island) growth mode starts from the smallest stable clusters nucleate on the substrate and each cluster grows independently into

three-dimensional islands. It usually happens when the film and substrate are dissimilar materials with large lattice mismatch. In the case of BFO-CFO on STO here, there are three kind of different materials to be stick together. The surface energy difference among them is the main factor that BFO-CFO on STO is following the Volmer–Weber (island) growth mode. It has been demonstrated that by choosing substrates with specific orientations, three types of vertically aligned nanocomposite (VAN) of BFO-CFO composite thin film can be obtained via Volmer-Weber growth mechanism.

The second type of film growth mode is the Frank–Van der Merwe or layer-by-layer growth mode which leads to the formation of planar sheets, because the extension of the smallest nucleus occurs in two dimensions. During depositing process, atoms are more strongly bonded to the substrate than to each other and the first layer is less strongly bonded than the previous layer. Those would be occur continuously until the bulk bonding strength is reach. BFO-CFO on STO could also proceed with this growth mode although they are different materials. BFO and STO substrate have same perovskite crystal structure, thus extention of the critical nuclei of BFO can occur in two dimension if the deposition parameters are carefully controlled. On the otherhand, to grow CFO on STO via layer by layer growth mode would be much more difficult to achieve, because the crystal structure is different.

The third mode is the Stranski–Krastanov mechanism, which is a combination of Volmer-Weber and Frank–Van der Merwe mode. The growth start with layer-by-layer growth for one or few monolayers, then it becomes energetically unfavorable and switches to island growth mode.

Following the simple thermodynamic model, the surface energy involved in the nucleation and growth of films can be analyzed and provide information for manipulating the film growth mode during deposition processes.
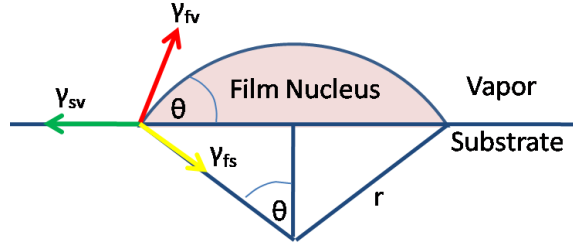
Figure 6. Cluster nucleation during deposition process [1].

Mechanical equilibrium (horizontal component) during nucleation process (Fig. 6.) could be described by Young's equation below, which explains the interfacial tension between the two phases (film and substrate) during vapor deposition.

$$\gamma_{sv} = \gamma_{fs} + \gamma_{fv}\cos\theta \qquad (1)$$

$$\cos\theta = \frac{(\gamma_{sv} - \gamma_{fs})}{\gamma_{fv}} \qquad (2)$$

γ_{sv} = substrate-vapor interfacial energy

γ_{fs} = film-substrate interfacial energy

γ_{fv} = film-vapor interfacial energy

θ = contact angle

For island growth, $\theta > 0$ therefore $\gamma_{sv} < \gamma_{fs} + \gamma_{fv}$. If γ_{fs} is neglected, this relation suggests that island growth occurs when the surface tension of the film exceeds that of the substrate. For BFO-CFO on STO vertically aligned nanocomposite thin film, the condition is that required by theVolmer–Weber island growth mode. The surface energy differences among different crystallographic orientations of several spinel and perovskite materials of interest in Table 1.

Table 1. Surface Energy of the Spinel and Perovskite Crystals [10].

structure	materials	surface energy (J/m²)		
		(111)	(110)	(001)
perovskite	SrTiO₃[18,20,22]	2.5	3.1,1.9,1.1	~1.0
	BaTiO₃[17,19]		2.23, 3.4,3.7,5.4	1.26
	PbTiO₃[19]	PbTiO₃[19]		0.97
				(most stable)
	MgSiO₃[21]	MgSiO₃[21]		2.2, 2.7
				(most stable)
spinel	CoFe₂O₄[23]	0.208	1.916	1.486
	NiFe₂O₄[24]	0.207	1.837	1.161
	Fe₃O₄[24]	0.223	2.164	1.451
	MgAl₂O₄[24]	0.298	2.702	1.446
				1.7, 3.0[28]

BFO-CFO vertically aligned nanocomposite (VAN) by PLD could occur because of the self assembled process between BFO and CFO in STO substrate. In fact, different VAN patterns of BFO-CFO can be obtained by using substrates with different orientations. Because of the difference in surface energy anisotropy, the morphologies of the BFO-CFO self-assembled nanostructures grown on (001), (110), or (111) STO substrates are significantly different. In that case, BFO could be pillar and CFO as the matrix or vice versa. For axample, on STO (001) substrate, BFO would be matrix, and CFO would be pillar. Whereas on STO (111) substrate, CFO will be matrix and BFO as the pillars; on STO (110) substrate, both BFO and CFO can form as either pillar or matrix depending on the actual condition used.

From simple thermodynamic models for the nucleation and growth of film materials, it is easy to understand how BFO became matrix and CFO became pillar or vice versa. As depicted in Fig. 7, BFO as perovskite has low surface energy when grown on STO (001)substrate because it has a corresponding equilibrium shape of a cube dominated by six {100} facets. In contrast, CFO as spinel has higher surface energy when grown on STO (001). Thus on STO (001), BFO and CFO have different wetting conditions, with BFO being easier to wet on the substrate surface. So, from wetting condition, BFO phase will easily cover almost the entire substrate while nucleation and growth of CFO will be hindered. As a result, CFO will lead to an inverted cone shape as the nuclei

of the partially wetting phase and grow into pillars with the correct area fraction [10]. Similarly in BFO-CFO grown on STO (111) substrate, CFO would be matrix and BFO becomes pillars, because the surface is reflected in an equilibrium shape of an octahedron bounded by eight {111} facets. While in the case of STO (110) substrate, both BFO and CFO have almost the same surface energy, thus they may form as a maze pattern.
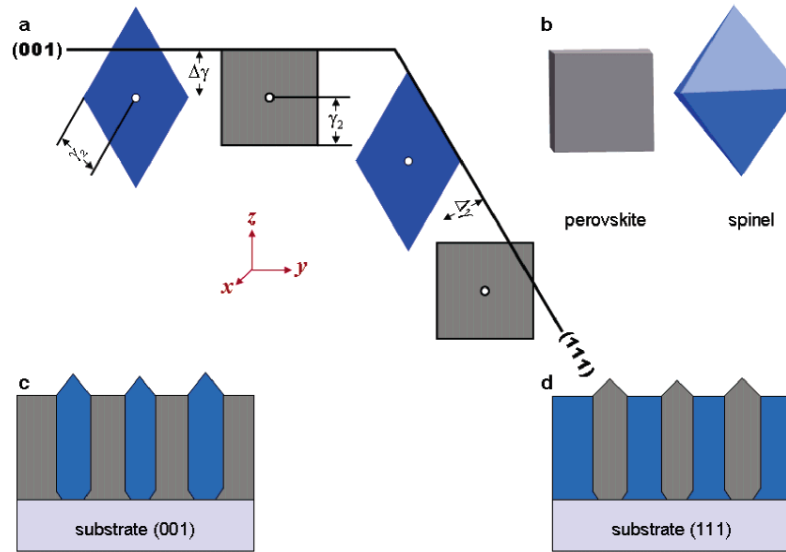
Figure 7. (a) Winterbottom construction, illustrating thechanges in nucleation modes for the perovskite and spinel on the (100) and (111) substrate. (b) Equilibriumshapes of a perovskite and a spinel. (c) Spinel forms nanopillars in perovskite matrix on a (001) substrate. (d) Perovskite forms nanopillars inspinel matrix on a (111) substrate surface [10].

For layer-by-layer growth, the film wets the substrate, hence $\theta \sim 0$ and therefore $\gamma_{sv} \geq \gamma_{fs} + \gamma_{fv}$. A special case of this condition is so-called homoepitaxy where the interface between substrate and film essentially vanishes and $\gamma_{fs} = 0$. For high quality layer-by-layer deposition one typically needs a film and substrate with only small differences in surface energy and in general materials with low surface energies will wet surfaces with higher surface energies. For Stranski–Krastanov growth initially $\gamma_{sv} \geq \gamma_{fs} + \gamma_{fv}$ is satisfied leading to layer-by-layer growth, but the build up of strain energy from lattice mismatch of film and

substrate can lead to a transition to island like growth typically after 5-6 monolayers [11].

In this research, fabrication of BFO-CFO on STO bilayer includes the Frank–Van der Merwe growth mode. Film growth becomes much like many processes in materials science, in that it is a nucleation and growth process. As film material deposits on the surface of the substrate, nucleation can occur in a number of ways, at step edges, defects, etc., and once the critical nucleus size is reached the growth of nucleus can occur in many ways. The growth is dependent on the kinetics of the system, the rate of adatom arrival, temperature, pressure, etc., and these are the tools that researchers use to control the growth of their materials.

The deposition parameters (e.g., laser energy density, frequency, and target-substrate distance in PLD), kinetics of system (e.g., the rate of adatom arrival, temperature, and pressure), and surface diffusivity need to be carefully controlled to get the films with the desired compositions, morphologies, and properties [12].

A. Effects of Temperature

In general, temperature affects mostly the thickness (growth rate) film, stoichiometry and crystallinity of the film and hence its ultimate properties [13]. In BFO-CFO on STO VAN, temperature will also affect the pillar size. Urgently effect of temperature is about impurity. In some researches of BFO-CFO on STO thin film, it could be observed that temperature could effect the film stoichiometry due to the presence of highly volatile Bi in the composition of BFO film. Consequently, temperature plays as the most critical parameter for the growth of stoichiometric single phase BFO films [14].

Impurity could appear in both low and high temperatures [15]. BFO formation is not stable because the atomic number of bismuth (83) and iron (26)

is quite different. It does not meet the criteria set by Pauling rules. Namely the configuration coordination of both Bi and Fe are not stable and match to each other. In addition, bismuth evaporates more easily than iron. So, right temperature needs to be considered to keep bismuth and iron to form BFO. In case BFO-CFO bilayer on STO, temperature will mostly effect the growth rate of each layer with possible introduction of impurities if wrong growth temperature was used.

In BFO-CFO on STO VAN, temperature range suitable for controlling the morphology of nanocomposites would be extremely narrow. Since BFO-CFO on STO VAN are formed by a self-assembled growth process of immiscible species, the control of the morphology is challenging. A first step would be the capability of controlling the pillar size for a particular composition. Temperature and deposition rate, determining surface diffusion and super-saturation of the adatom, are essential for controlling the pillar size [16]. Researches have shown that progressive loss of Bi as the temperature increases, and at high temperatures no Bi incorporates into the films. The evaporation of Bi frequently causes diminution of the BFO phase and leads to the formation of Fe_xO_y secondary phases.

B. Pressure Effect

The gas pressure in the chamber (working pressure) also has decisive effect on the occurrence of the phase separation behavior and properties of the perovskite–spinel composites. In BFO-CFO bilayer, it was found that good phase separation occurred at high temperatures and slow growth rate. In practice, higher working pressure always leads to slower growth rate.

Similar conclusions were reached in BFO-CFO nanocomposite growth on STO. In another research, it has been reported that not only the phase separation of the composite films occurred at high temperature and slow growth rate, but

also the size of nanopillars increased with increasing substrate temperature and/or decreasing growth rate [16]. This agrees with the report where the phase separation of the perovskite–spinel composite film was clearly observed when the growth rate was reduced by decreasing the substrate temperature or the pulse repetition rate. It is clear that, pressure, temperature and repetition rate are the intimately related parameters in PLD film growth process.

C. Pulse Laser Energy and Repetition Rate

The energy and repetition rate used in PLD system directly affect the energy and amount of the incident adatoms reaching the substrate. Higher pulse laser energy and repetition rate would provide more incident adatoms with higher kinetic energy when the adatoms reach the substrate. Thus, by controlling these parameters one can control the growth rate and phase separation. For BFO-CFO multilayer grown on STO, we need to consider the two-dimensional extension of the smallest nucleus. Its means that atoms must be more strongly bonded to the substrate than bond to each other. Thus, these conditions, pulse laser energy and repetition rate needed to be optimized to satisfy.

In nanocomposite BFO-CFO on STO case, small island building blocks need to occur first, meaning that bonding among films atoms has to be stronger than to substrate. In this case, higher pulse laser energy and large repitition rate are usually needed for obtaining good phase separation. Nevertheless, it is noted that other deposition parameters have to be taken into account simultaneously when trying to optimize the film growth processes.

2.2 Basic Properties of BFO and CFO

2.2.1 Multiferroicity

Multiferroicity is combination between magnetic, ferroelectric, and ferroelastic properties. Materials simultaneously posses two or more of the so-called "ferroic' order parameter-ferroelectricity, ferromagnetism, and

ferroelasticity are called multiferroics. Magnetoelectric coupling typically refers to the linear magnetoelectric effect or the induction of magnetization by an electric field or polarization by a magnetic field [8]. The promise of coupling between magnetic and electronic order parameters and the potential to manipulate one through the other has captured the imagination of researchers worldwide. The ultimate goal for device functionality would be a single-phase multiferroic with strong coupling between ferroelectric and ferromagnetic order parametersmaking for simple control over the magnetic nature of thematerial with an applied electric field at room temperature.
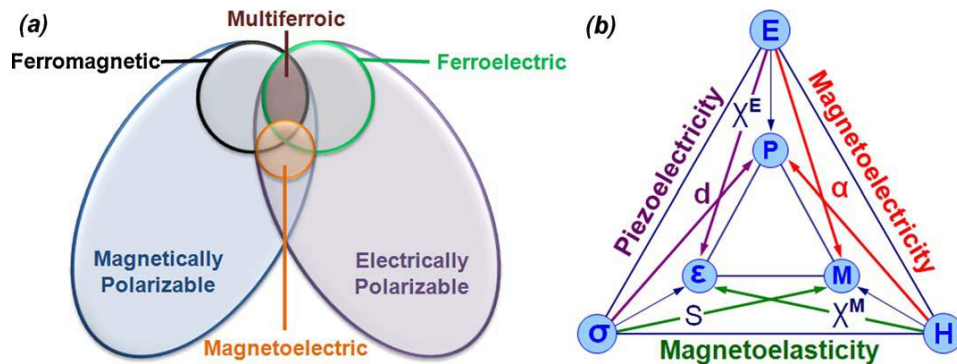
Figure 8. Multiferroic and magnetoelectric materials [1].

In Figure 8, (a) Relationship between multiferroic and magnetoelectric materials. Illustrating the requirements to achieve both in a material [17]. Figure (b) Schematic of different types of coupling present in materials. Much attention has been given to materials where electric and magnetic order is coupled. These materials are known as magnetoelectric materials [1].

2.2.2 Magnetic Properties

Antiferromagnetic and ferromagnetic is related to the spin direction. Antiferromagnetic materials have spin direction alligning in a regular pattern with neighboring spin pointing in opposite directions. In contrast, in ferromagnetic materials, the spins are pointing along the same direction and from a long-range ordering.
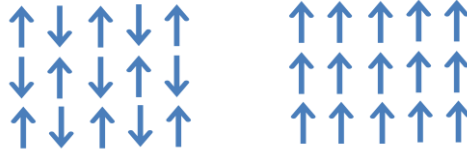
Figure 9. Antiferromagnetic (left) and ferromagnetic (right).

BFO is a typical antiferromagnetic material with a Něel temperature T_N=653 K. Since antiferromagnetism can couple to ferromagnetism, for instance, through a mechanism known as exchange bias in, which ferromagnetic film is either grown upon the antiferromagnetic or annealed in an aligning magnetic field, causing the surface atoms of the ferromagnetic material to align with the surface atom of the antiferromagnetic. This provides the ability to pin the spin orientation of a ferromagnetic film, which is the basis of magnetic sensor.
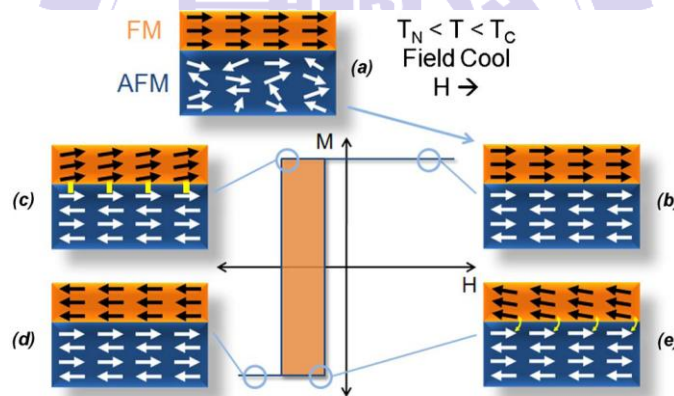
Figure 10. Schematic diagram illustrating the various stages of spin configuration in an exchange bias heterostructure being magnetically cycled. The diagrams show the spin configuration (a) above T_N under an applied magnetic field H, (b)–(e) below T_N at different applied magnetic fields [18].

Perhaps, exchange bias, more than any other single effect, has played the biggest role in the development of modern magnetic materials. When heterostructures with a ferromagnet are placed in contact with an

antiferromagnet and are cooled through the Něel temperature (T_N) of the antiferromagnet (with the Curie temperature, T_C, of the ferromagnet larger than T_N) in the presence of an applied magnetic field, an anisotropy is induced in the ferromagnetic layer. Exchange bias is one of a number of phenomena observed at the interface between an antiferromagnet and a ferromagnet [18].

2.2.3 Electric Properties

BFO also has interisting electric properties, especially its dielectric properties. To understand dielectric properties, polarization should be defined. When a dielectric is placed in an electric field, electric charge do not flow through the material as they do in a conductor, but only slightly shift from their average equilibrium position causing dielectric polarization.
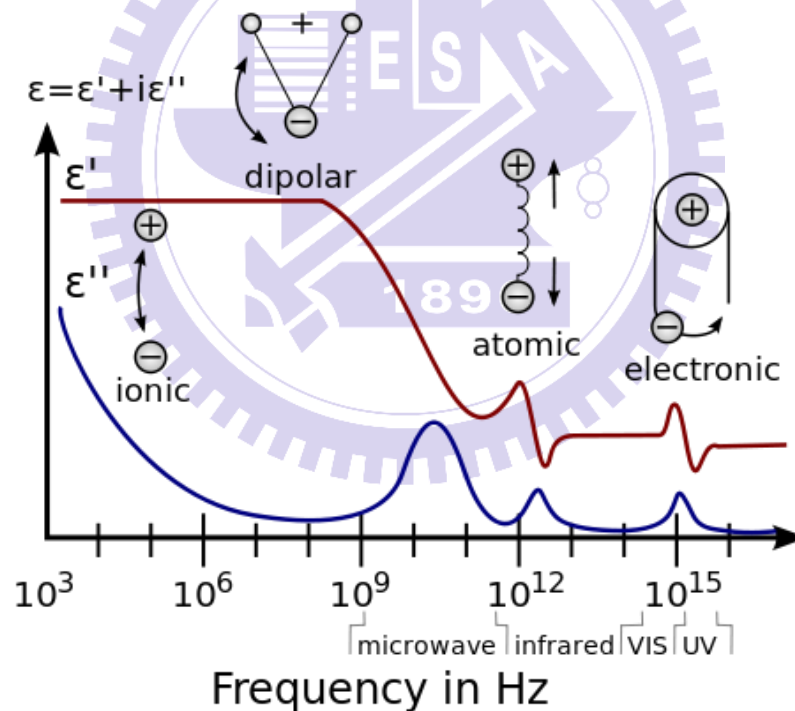
Figure 11. Types of electric polarization [19].

Because of dielectric polarization, positive charges are displaced toward the field and negative charges shift in the opposite direction. This creates an internal electric field that reduces the overall field within the dielectric it self. If

a dielectric is composed of weakly bonded molecules, those molecules not only become polarized, but also reorient so that their symmetry axis aligns to the field. There are four kind of polarization, electronic polarization, ionic polarization, dipolar polarization and space charge polarization as depicted schematically in Fig. 11. A dielectric material is an electrical insulator that can be polarized by an applied field. In BFO we could find two kinds of polarization. Namely, electronic polarization, due to lone pair of electrons in bismuth atom and ionic polarization originated from primitive rombohedral structure in perovskite structure crystal of BFO.

Dielectric properties also related to capacitance measurement. Capacitance can be calculated if the geometry of the conductors and the dielectric properties of the insulator between the conductors are known. A qualitative explanation for this can be given as follows. As a quantitative example consider the capacitance of a parallel plate capacitor constructed by two parallel plates both of area and separated by a distance d:

$$C = \varepsilon_r \varepsilon_0 \frac{A}{d}$$
(3)

Here ε_r is the relative static permitivity and ε_0 is the permitivity of vacuum ($\varepsilon_0 \approx 8.854 \times 10^{-12}$ F m^{-1}). BFO is an electrical insulator, the electric polarization of BFO, can be evaluated by dielectric and capacitance measurements. Because BFO is electrical insulator, so that electric resistance for BFO is very high.

2.2.4 BFO and CFO Properties in Below Temperaure

Generally, antiferromagnetic order may exist at suffeciently low temperature, vanishing at and above a certain temperature, or the Něel temperature T_N. Above the Něel temperature, the material is typically paramagnetic. Neel temperature or magnetic ordering temperature is the temperature above which an antiferromagnetic or ferrimagnetic material become paramagnetic, that is the thermal energy beocmes large enough to destroy

macroscopic magnetic ordering within the material. The Nĕel temperature is analogous to the Curie temperature for magnetic material.
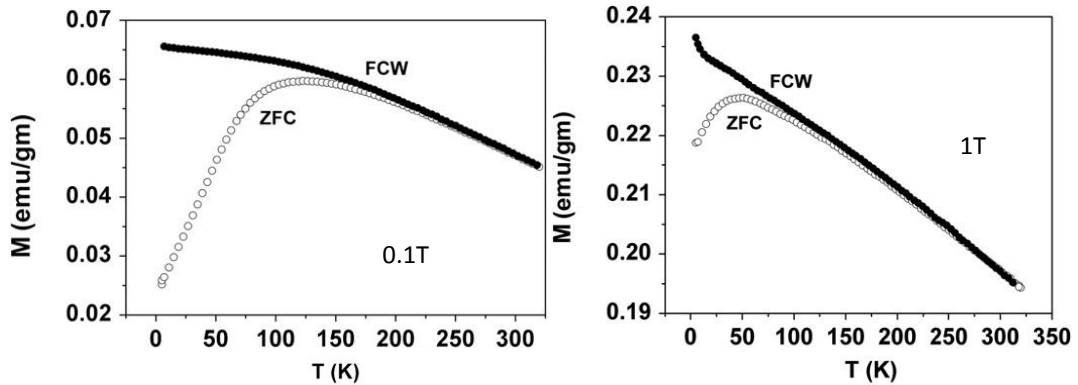
Figure 12. M-T measurement for BFO powder single crystal [7].

For BFO, although T_N=653 K has been clearly indentified, however, as shown in Fig. 12, there is magnetic phase transition observed at low temperatures. The magnetic phase transition is related to the antiferromagnetic domain pinning effect. Increasing magnetic field will increase allignment of momen magnetic, so that the magnetic phase transition was shifted to lower temperatures because of the antiferromagnetic domain pinning effect was changed.

In addition to those observed in the M-T curve, magnon measurement also found anomalies at usual temperature. Figure 13 shows the Raman measurement of BFO which clearly displays phase transitions at ~140 K and ~200 K. The origin of which is as yet unclear but has been tentatively attributed to spin reorientations. The above right figure indicates that magnon linewidth narrows near 140 K, suggesting the features of "critical slowing down" of spin fluctuations. The cross section divergence cannot come from impurities. Moreover, as shows in the lower right figure of Fig. 13, preliminary electron paramagnetic resonance measurements also shows clear anomalies at 140 K and 200 K.
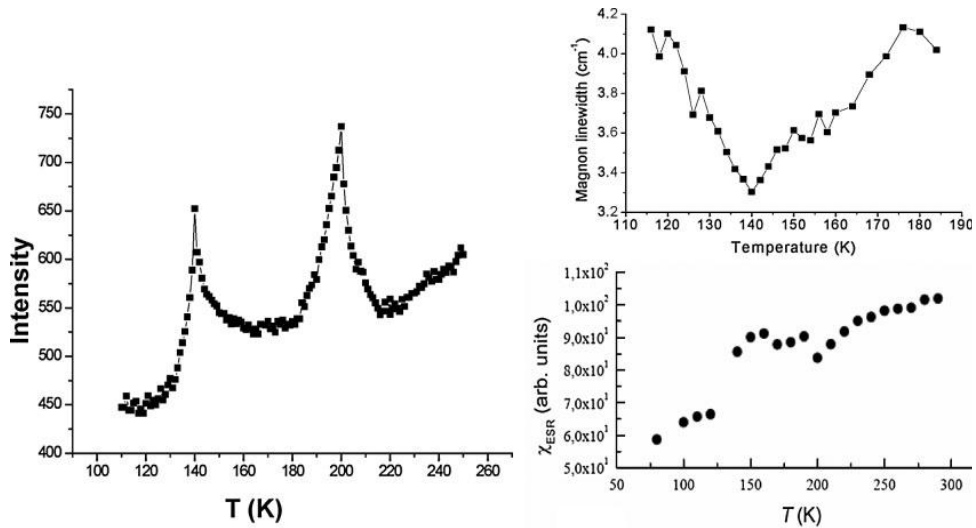
Figure 13. Intensity of magnon peaks in the Raman spectra as a function of temperature [20].

Dielectric measurement also displays similar low temperature anomalies in BFO. BFO is piezoelectric at all temperatures below 1100 K, any magnetoelastic phenomena at its magnetic-phase transitions are apt to create responses in the dielectric response. In Figure 14, the subtle low-temperature anomalies at 215 K, 140 K and 55 K coincide with the temperatures where magnetic, magneto-optic and elastic anomalies have been seen. Nevertheles, none of the dielectric anomalies is strong and, curiously, none seems to affect the dielectric loss.
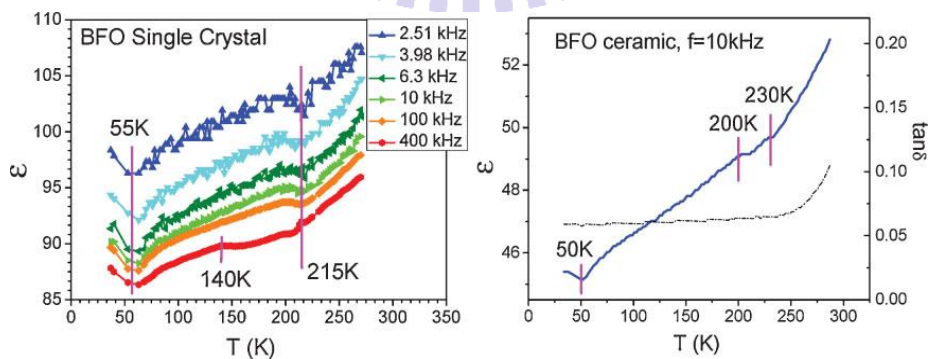
Figure 14. dielectric measumerent from BFO [4].

Anomalies in the relative dielectric constant (ε), is possibly due to coupling to magnetic (or magnetoelastic) transitions at low temperature. The anomalies

do not seem to affect the dielectric loss (tan δ) [4]. Their weakness shows that they do not correspond to ferroelectric phase transitions, but arises instead from weak coupling to another order parameter, most likely magnetic. Additional dielectric and conductivity anomalies ware reported [21] at T_N=643 K (370 °C), clearly related to magnetoelectric coupling, and magnetodielectric coupling is also responsible for the reported anomaly in the birefringence of BFO at T_N [22]. Another anomaly was reported at mysterious transition at 458 K, although this dielectric anomaly may it self be an artifact caused by the change in resistivity [9, 22-24].

Resistance measurement in the temperature regime also reveals some aspects of magnetoelectric properties. As shown in Figure 15, the resistance for BFO displays a clear insulating beharvior as function of temperature. However, under external applied magnetic field, magnetoresistance at low temperatures is clearly revealed, indicating possible magnetoelectric coupling at low temperature.
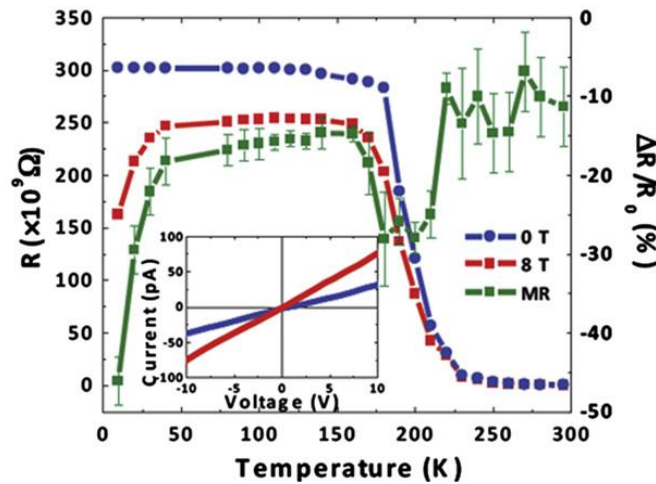
Figure 15. Magnetotransport study on BFO 109° domain Wall. Resistance - temperature curves at two different external magnetic fields, 8 T (red) and 0 T (blue) and the corresponding magnetoresistance (green) [25].

More detailed analysis on the data shown in Fig. 15, indicated that the MR is directly related to the preferential transport parallel to the ferroelectric domain

walls. The temperature - dependent resistance and I-V behavior of similar devices were also measured under two different magnetic fields, 0 T and 8 T (blue and red curves in Figure 15), respectively, the inset shows linear I-V plots with and without the magnetic field. Negative MR is only observed for temperatures below the transition temperature (~200 K), which suggests that magnetic interactions are likely to play a key role in influencing the observed transport behavior. Moreover, below 40 K, the magnitude of MR gets significantly larger, from ~20% at ~100 K to ~60% at ~10 K [25].

From the above discussion it is apparent that substential magnetoelectric coupling exist in BFO at low temperatures. Thus, combination BFO with ferromagnetic CFO interisting to observed, especially when both are in nanoscale. However, before we explore the possible coupling between antiferromagnetic-ferroelectric BFO and ferromagnetic CFO, we first introduce briefly properties of CFO it self.

Figure 16, shows the zero-field-cooled and field-cooled (ZFC/FC) magnetization curves of the as-prepared $CoFe_2O_4$ samples measured at temperatures between 10 K and 330 K with an applied field of 100 Oe.
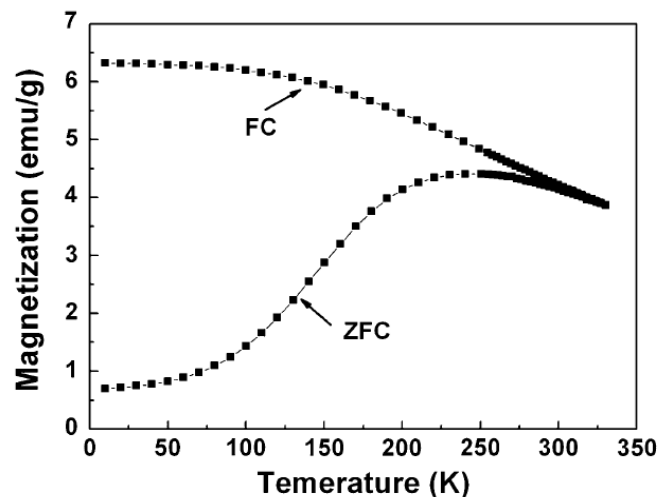
Figure 16. Zero-field-cooled (ZFC) and field-cooled (FC) curves for the as-synthesized $CoFe_2O_4$ nanoparticles under an applied magnetic field of 100 Oe [26].

As the temperature rises from 10 K to 330 K, the ZFC magnetization increases first and then decreases after reaching a maximum at 240 K, which is correspond to the blocking temperature (T_B). This result further proves that the $CoFe_2O_4$ displays a superparamagnetic behavior at room temperature [26]. Whereas the FC magnetization decreased endlessly as the temperature increased. It is argued that the difference between ZFC magnetization and FC magnetization below T_B is caused by energy barriers of the magnetic anisotropy [27].

From the interisting properties observed in BFO and CFO in the below room temperature regime, it will be the key to explore the possible of magnetoelectric and ferromagnetic-antiferromagnetic coupling that might be occur when combining the two materials with designed structures.
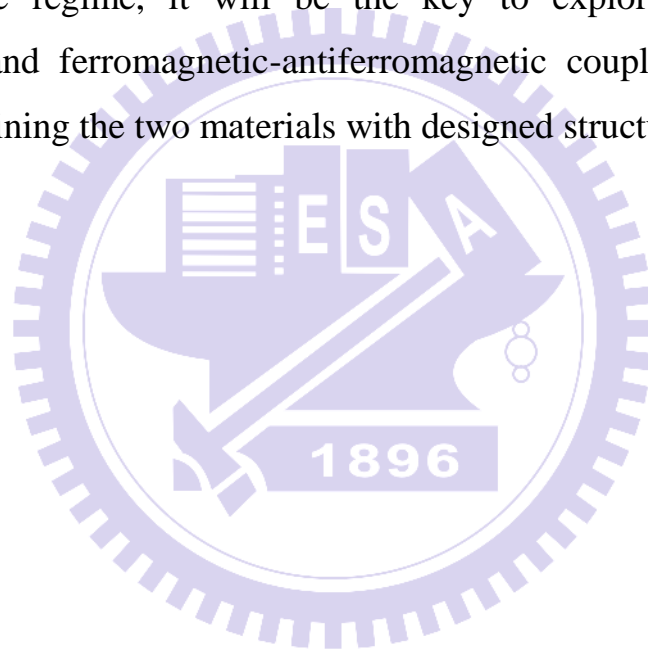
III. Experiment

3.1 Solid State Reaction

In this research, solid state reaction was used to make BFO and CFO bulk target and these bulk target ware used to make BFO-CFO thin film. To make BFO and CFO target from BFO and CFO powder by solid state reaction, precise calculation of chemical reaction of each basic material should be done. Generally, type of bismuth and iron material to make BFO is bismuth oxide (Bi_2O_3) and ferrit oxide (Fe_2O_3). Calculation of chemical reaction from Bi_2O_3 and Fe_2O_3 can be described by; For example:

$$\text{Mass of } Fe_2O_3 = 1 \text{ gram}$$

$$\text{Mr } Fe_2O_3 = (2 \times \text{Ar Fe}) + (3 \times \text{Ar O})$$

$$= (2 \times 55{,}845) + (3 \times 15{,}99) = 159{,}66 \text{ gram/mol}$$

$$\text{Mol } Fe_2O_3 = \frac{\text{Mass } Fe_2O_3}{\text{Mr } Fe_2O_3} = \frac{1}{159{,}66} = 0{,}0062633 \text{ mol}$$

$$\text{Mol } Bi_2O_3 = \text{Mol } Fe_2O_3 = 0.0062633$$

$$\text{Mr } Bi_2O_3 = (2 \times \text{Ar Bi}) + (3 \times \text{Ar O})$$

$$= (2 \times 208{,}98) + (3 \times 15{,}99) = 465{,}93 \text{ gram/mol}$$

$$\text{Mass of } Bi_2O_3 = \text{Mol } Bi_2O_3 \times \text{Mr } Bi_2O_3$$

$$= 0.0062633 \times 465{,}93 = 2{,}918 \text{ gram}$$

After that, mixed precise mass of Bi_2O_3 and Fe_2O_3 by using agate mortar with aceton and dried at 100°C for 2h. After grinding, the mixed powder sintered at 600°C for 4h thus continued by 880°C for 480 second. Do grinding process again, thus sample ware pressed uniaxially (500 Mpa) into pellets and annealed in furnace at 600°C for 12 hours. For CFO, calculation was done similarly as that used to get $BiFeO_3$ powder. However, in this case CoO and Fe_2O_3 powder ware used to prepare $CoFe_2O_4$ powder, the powder was dried and

ground, then calcined at 1000°C for 12 hours. Finally, it was pressed into pellets and annealed at 1000°C for 12 hours.

The XRD result shown in Fig. 17 (a) and 17 (b) evidently confirmed that the target obtained by the processes describe above were indeed of single phase materials with correct stoichiometry.
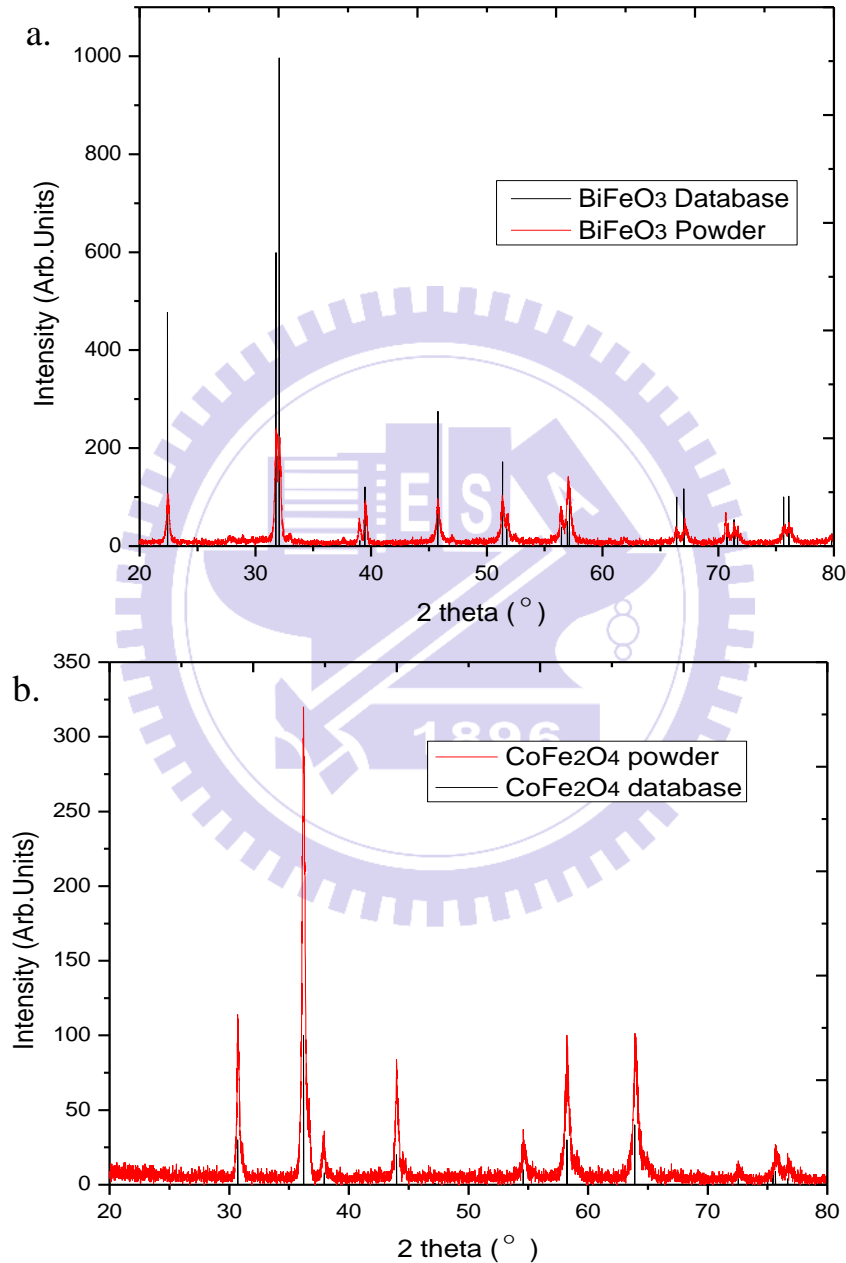
Figure17. $BiFeO_3$ and $CoFe_2O_4$ XRD pattern.

It is noted that heat treatment process is very important in this experiment. Although the temperatures were chosen according to the phase diagram and

parameters reported in the literature, we note that in order to get good quality samples, environmental conditions should be considered as well.

3.2 Pulse Laser Deposititon

The set up of the PLD system is schematically illustrated in Fig. 18. Briefly, it contains a laser generation system and a vacuum chamber with substrate and target holders.
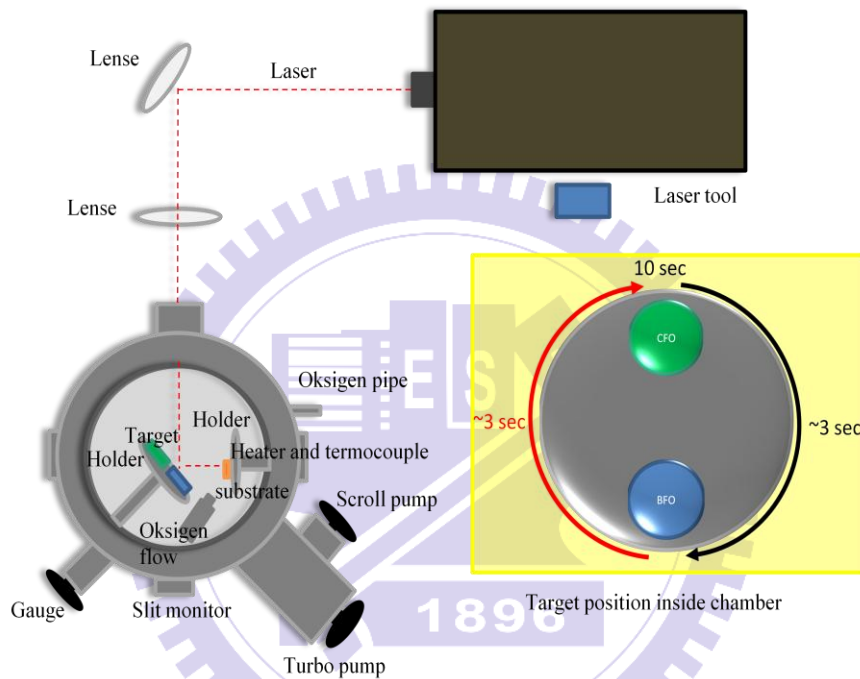
Figure18. Schematic of PLD experiment set up.

The vacuum chamber should be able to reach a base preseure of 10^{-7} mT which is acheive by sequential pumping using scroll pump and turbo pump. A gauges and oksigen pipe were equiped to control pressure inside the chamber. In this study, the BFO-CFO film on STO substrate were deposited at an oxigen pressure 50 mT to 200 mT depending on what surface desired and how thick the film will be both substrate temperature and deposition time were further optimazed. The chamber also has heater and thermocouple to control the temperature used to make samples.

In further controls on the deposition process were accomplished by tuning the laser pulse energy, repetition rate direction and focus of the laser beam with lenses direct to chamber. Beside the main conditions in PLD system, we can also control the rotation of target and the distance between substrate and target to optimize the conditions for making good quality samples. Distance between target-substrate will affect the incident adatom from target coming to substrate. If closer distance was predicted the incident adatoms are more abundant than that obtained if larger target-substrate distance was used within the same deposition time is rich than far distance in the same deposition time.

For BFO-CFO vertically alligned nanocomposite fabrication, two targets were used simultaneously. There are several ways to make BFO-CFO vertically alligned nancomposite. The popular way is to use single target made BCFO mixtures. BCFO target is a combination of BFO powder and CFO powder, where there is no chemical reaction between mixed BFO and CFO. Such that, BFO and CFO particles will be separated during deposition process and self assembled into nanocomposite. Howerver, in order to gain more control on the microstructure, in this reseach we used two targets to make BFO-CFO nanocomposites.

The deposition time for each target is important in fabrication of BFO-CFO vertically alligned nanocomposite by using two targets. In this case,we need to know how much deposition time is needed to build single three-dimensional islands first. Because, further growth of island will result in nanopillars embedded in matrix until nanocomposite pattern is accomplished. For BFO-CFO on STO (001), CFO would be pillar, so in that case we need to consider the duration of deposition time to make the first single CFO islands. After CFO was deposited, the BFO deposited on the STO (001) substrate will form a continous matrix because of the smaller lattice mismatch between them.
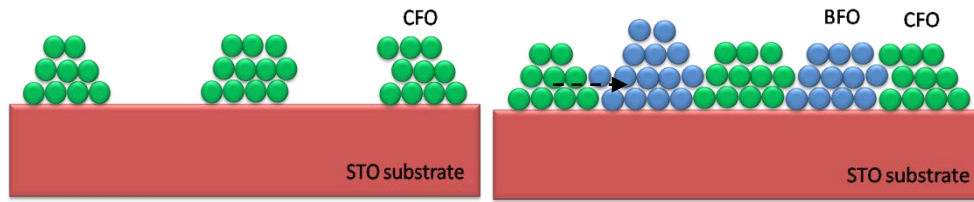
Fig. 19. Deposition step and time duration selected for forming BFO-CFO vertically aligned nanocomposite.

In this case, a 5-15 second deposition time combination is appropriate with total a deposition time of 30 minute. It was found that if the deposition time of CFO step is longer than 15 second, pillars cannot be constructed and film tend to collapse into layer. The 30 minutes total deposition time correspond to 180 time cycle for each target if 10 second for each target is used.

3.3 Characterization

The microstructure and physical properties of the obtained samples were characterized by XRD, scanning electron microscope (SEM), superconducting quantum interference device (SQUID), and impedance analyzer or (LCR meter), respectively.

3.3.1 X-ray Diffraction (XRD)

XRD characterization is due essential to identify the phases formed in the obtained films. The Bragg's law gives the angles for coherent and incoherent scattering from a crystal lattice, which describes the relations between the wavelength (λ),diffraction angles (θ), and the lattice spacing between certain planes of the crystalline phases inside the film by the following relation :

$$2d\ sin\theta = n\ \lambda \qquad (4)$$
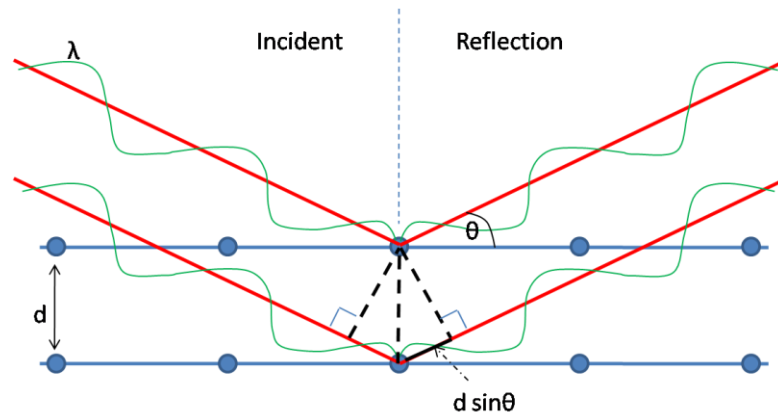
Figure 20. Schematic of the Bragg's law.

Thus, from the diffraction peak, one can confirm the crystal structure of the material in study. In this research, XRD also used to investigate strain effect in the sample. BFO, CFO and STO have different lattice constants, resulting in strain effect among them when they are in proximity. Especially in the case of BFO-CFO on STO VAN, the BFO has a compressive in-plane strain due to the lattice mismatch with STO substrate. In addition, BFO also has a compressive strain along out-of plane direction due to the lattice mismatch with the CFO. Strain effect in BFO due to lattice mismatch with STO and CFO makes the XRD peaks of BFO in BFO-CFO/STO VAN thin film shift as compared to that of the BFO powder.

Lattice constant of BFO was change because those strain effect which make X-ray diffraction also change. According to Bragg's law, angle of reflection beam (θ) will change if spacing between diffracting planes (d) was changed. where d is also indicated as a lattice constant in the sample. So, when lattice constant of BFO was changed to higher or lower value caused lattice mismatch among BFO, CFO and STO, so angle of reflection beam (θ) also will be changed which will be evidence by shift of the BFO peak in diffraction pattern of XRD result.

3.3.2 Scannng Electron Microscope (SEM)

SEM was used to identify sample microstructure. In this research SEM was also used to reveal both the surface and cross sectional structures, especially for BFO-CFO on STO VAN to indicate nanocomposite structure. SEM is a type of electron microscope to take an images from the sample surface by scanning it with a high-energy beam of electrons. In SEM, electrons are emitted from a tungsten filament cathode and accelerated towards an anode. There are lenses to focus the beam to have spot radius from 0.4 μm to 5 μm. The electron beam will interact with the sample and its interaction volume can extend from less than 100 nm to around 5 μm into the surface. Pairs of scanning coils deflect the beam horizontally and vertically make a rectangular area scan in the sample surface.
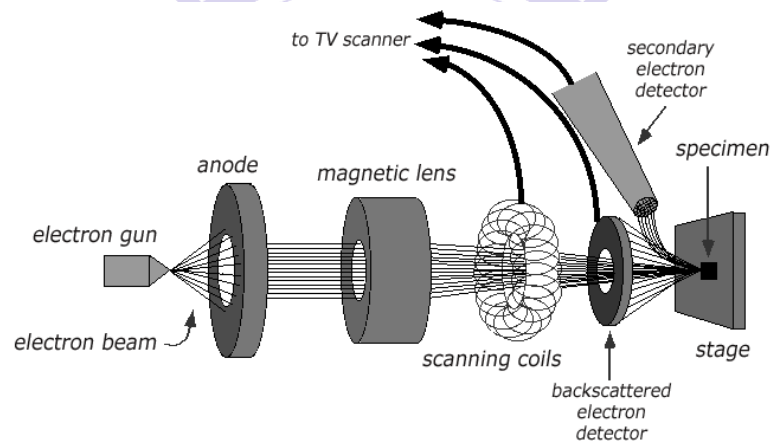
Figure 21. Schematic illustration of a SEM (rotated by 90° counter-clockwise) [28].

Imaging can be achieved through the detection of low energy (< 50 eV) secondary electrons, or backscattered electrons. The latter consist of high-energy electrons originating in the electron beam, that are reflected or back-scattered out of the specimen interaction volume. Backscattered electron imaging is useful for distinguishing one material from another, since the yield of the collected backscattered electrons increases monotonically with the specimens atomic number. Backscatter imaging can distinguish elements with atomic number differences of at least three, i.e., materials with atomic number

differences of at least three would appear with good contrast on the image. Because these electrons are emitted from a depth in the sample, the resolution in the image is not as good as that obtained from the secondary electrons, with a beam resolution ranging from 10 to 20 nm [28].

3.3.3 Atomic Force Microscopy (AFM)

AFM is a scanning probe microscope tool to image and measure a material in nanoscale. In AFM consist of a microscale cantilever with an atomically sharp tip, used to scan material surface. The tip could produce a Coulomb repulsive force from deflection of the cantilever according to Hooke's law. Then, it will effect to laser spot reflecting in photodiodes. To maintain a constant tip-to-sample distance, a feedback loop is implemented between the photodetector and the cantilever. The cantilever is maintained fixed in a tip holder, and the sample placed on top of a piezoelectric column that can move in the z direction for height adjusting and in the x, y directions for surface scanning [28].
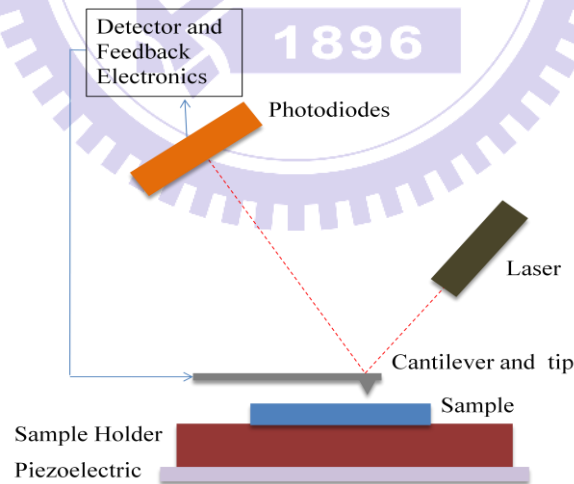

Figure 22. Schematic of an AFM.

Two scanning modes, namely contact mode and resonace mode are commonly used in AFM operation. In the contact mode, the force between the tip and the sample is kept constant by the feedback loop by maintaining a

constant cantilever deflection. While in resonance mode, the cantilever is driven to oscillate near its resonance frequency by a small piezoelectric element mounted in the tip holder; the oscillation amplitude is modified as a result of tip-sample forces, so that the reflected laser beam is deflected in a regular pattern over the photodiode array, generating a sinusoidal electronic signal which is modified by the oscillation amplitude variation.

Depending on the height of the tip above the sample, different forces such as electrostatic interaction, magnetic forces, Van Der Waals attraction, water adhesion and Coulomb repulsion can play a role. If the cantilever enter intermittently into contact with the surface, the technique is known as tapping mode; otherwise, it is referred to as non-contact mode.

3.3.4 Superconducting Quantum Interference Device (SQUID)

SQUID has been widely used to measure magnetic properties of material. The SQUID devices is due to the Josephson effect exhibiting in two parallel Josephson junctions consisting of two superconductors separated by a thin insulating layer. The device allows a change of magnetic field associated by one flux quantum to be measured. The flux which associated by Josephson junctions is quantized in units of flux quantum $\phi_o=2.07 \times 10^{-15}$ T.m^2.
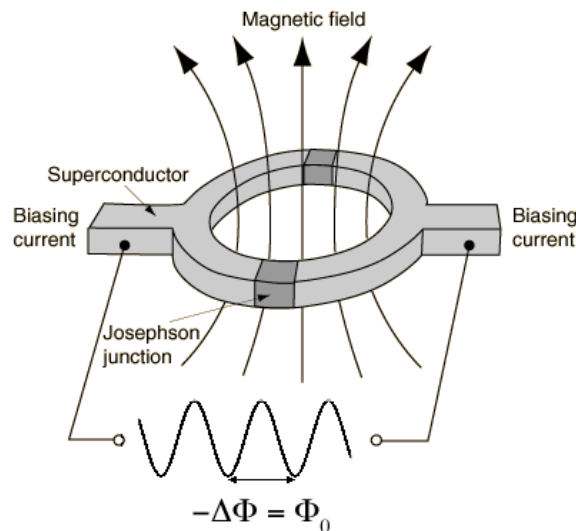
Figure 23. Schematic illustration of a SQUID [28].

SQUID is operated with a constant bias current, thus the measured voltage oscillates with the phase changes between the two junctions, which depends upon the change in the magnetic flux, as illustrated in Figure 23. Detecting this circulating current enables the use of the SQUID as a magnetometer.

3.3.5 Impedance analyzer (LCR meter)

LCR meter is an equipment to measure the inductance (L), capacitance (C) and resistance (R) in material. In this research, LCR meter was used to measure and analyze electric properties of BFO-CFO on STO substrate especially capacitance and resistance dependence on temperature. For capacitance measurement, two probe is enough to get capacitance value of the sample. DC volatge drop will build across the sample, thus temperature dependent capacitance of the sample could be obtained. For resistance measurements, both two probe and four probe methode were used.
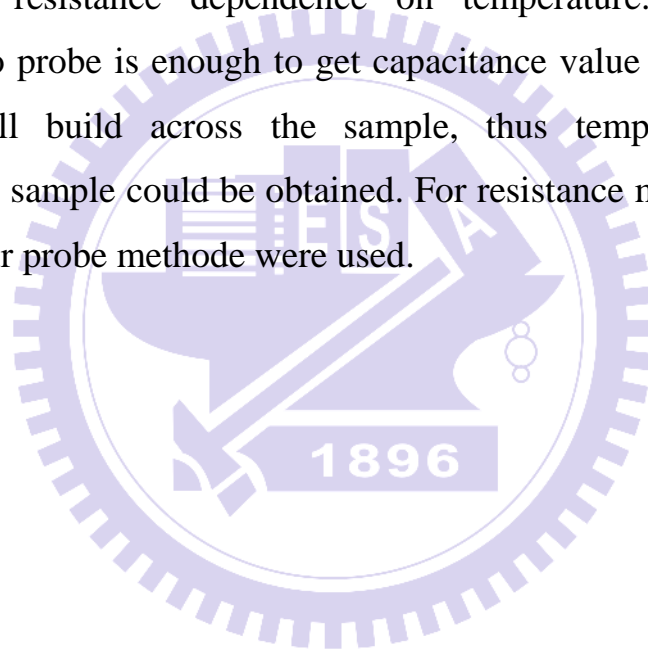
IV. Results and Discussion

4.1 Structure Analysis

In this research, three kinds of BFO-CFO vertically align nanocomposite were fabricated according to substrate direction. As shown in the Fig. 24, the temperature suitable fo growing the BFO-CFO nanocomposite film are 600°C, 650°C, and 700°C. Below 600°C, BFO growth was not good, i.e. only amorphous film were obtained at T=550°C (Fig. 24). On the other hand, for temperature higher than 700°C, bismuth was very easy to evaporate, making the stochiometry of the sample unstable and may even leading the formation of impurity phases, such as Fe_2O_3 and Bi_2O_3.
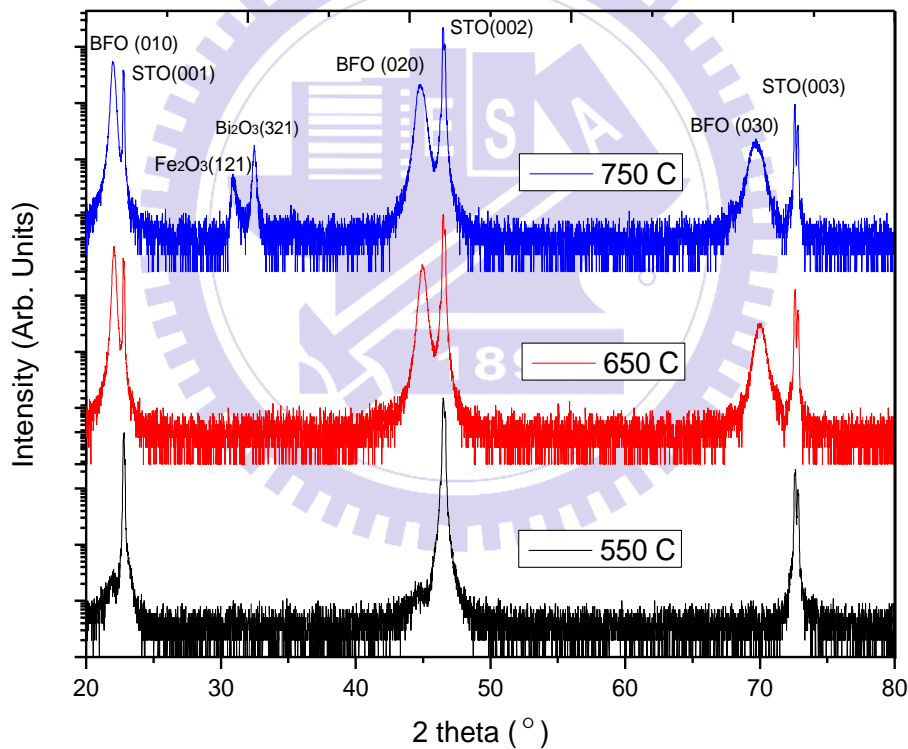

Figure 24. XRD pattern of BFO thin film on STO (001) substrate with different temperature growth conditions.

Deposition condition, such as pressure, repetition rate, and pulse energy are also dependent on the temperature used. In general, with the same growth temperature, BFO is more difficult to grow at higher pressure than in the low

pressure. The thickness of BFO also depend on repititon rate. In present experiment, pressure at around 100 mT-250 mT and repitition rate at 5 Hz-10 Hz were found appropriate to grow BFO on STO. The pulse energy, not only will affect to the final film thickness, but also the formation of the impurity phase. Higher energy densities often caused more BFO to decomposed. In this reseach pulse energy for growing BFO on STO was optimized to within 250 mJ-350 mJ.

In this research we used separated BFO and CFO target to fabricate BFO-CFO thin films, consequently, the condition for growth of individual phase have to be established first. Generally, CFO needs higher growth temperature than BFO, because CFO and STO have different crystal structures. In contrast, BFO is having the structure crystal same with STO. Thus, BFO is easier to growth on STO. moreover, lattice mismatch between BFO-STO is smaller than that of CFO-STO, which also plays an important role in searching for optimal growth condition.
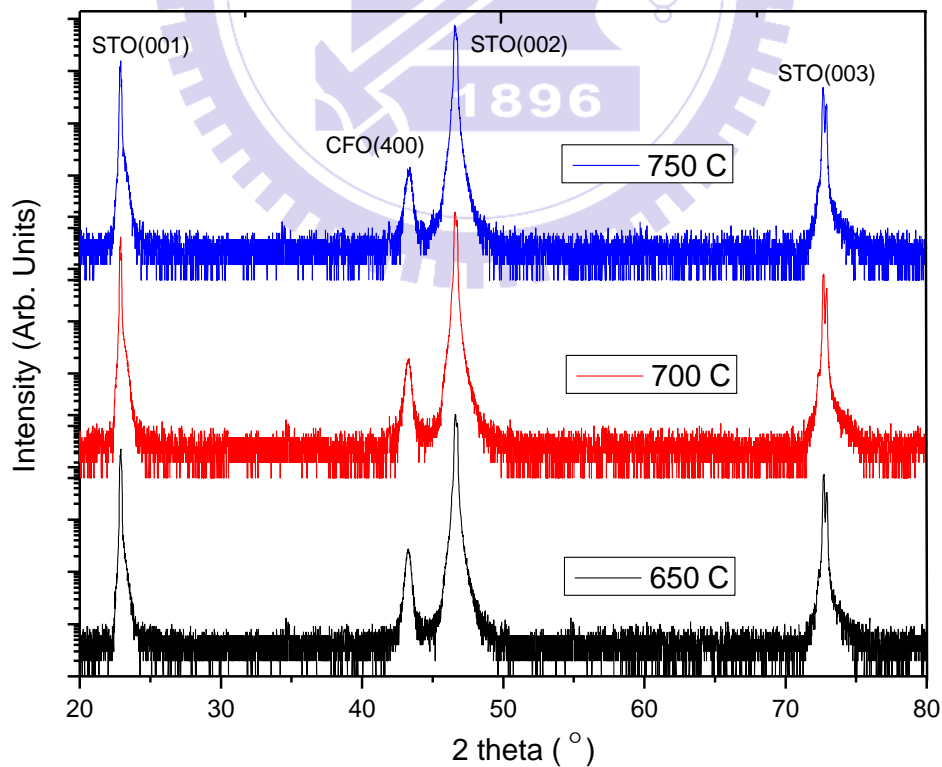
Figure 25. XRD pattern of CFO thin film on STO (001) substrate with different growth temperatures.

As is evident from Fig. 25, single phase CFO can be grown on STO at temperature of 650 ^{o}C, 700 ^{o}C, and 750 ^{o}C, with pressure condition around 100 mT-200 mT, repetition rate of 5 Hz-10 Hz and pulse energy at 250 mJ-350 mJ, respectively, these conditions are almost the same as those needed for depositing BFO on STO with our PLD system. Impurity in CFO was relatively difficult to appear, because CFO is more stable and needs higher temperature to decompose into CoO and Fe$_2$O$_3$. Therefore, almost the same conditions growth were used to make the BFO-CFO composite film on STO, even with two separate target.

Since the wetting condition for BFO and CFO are different, when BFO and CFO are growing on STO substrate at the same time, they will self essemble to form composite epitaxial thin films. Fig. 26 displays a collections of XRD result for BFO-CFO/STO (001), (011), (111) VAN, BFO/CFO/STO (001), (011), (111) bilayer, BFO/STO (001), (011), (111) single layer, BFO powder and CFO powder, respectively.
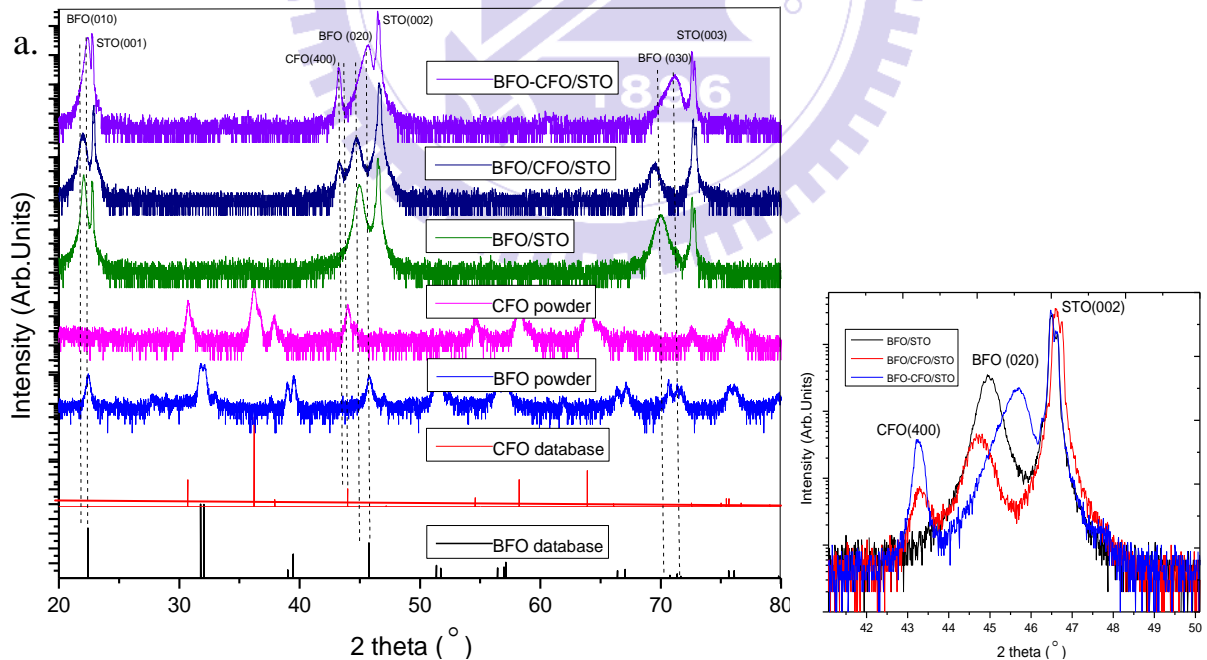
Figure 26. XRD from BFO-CFO/STO VAN, BFO/CFO/STO bilayer, BFO/STO single layer, BFO and CFO powder grown on STO with different orientations. a. (001), b. (011), c. (111).

From the XRD results, it is evident that the diffraction peaks of BFO and CFO films are slightly shifted as compared to that of data base as well as BFO and CFO powders. The shifts indicated that there are substantial strain effects

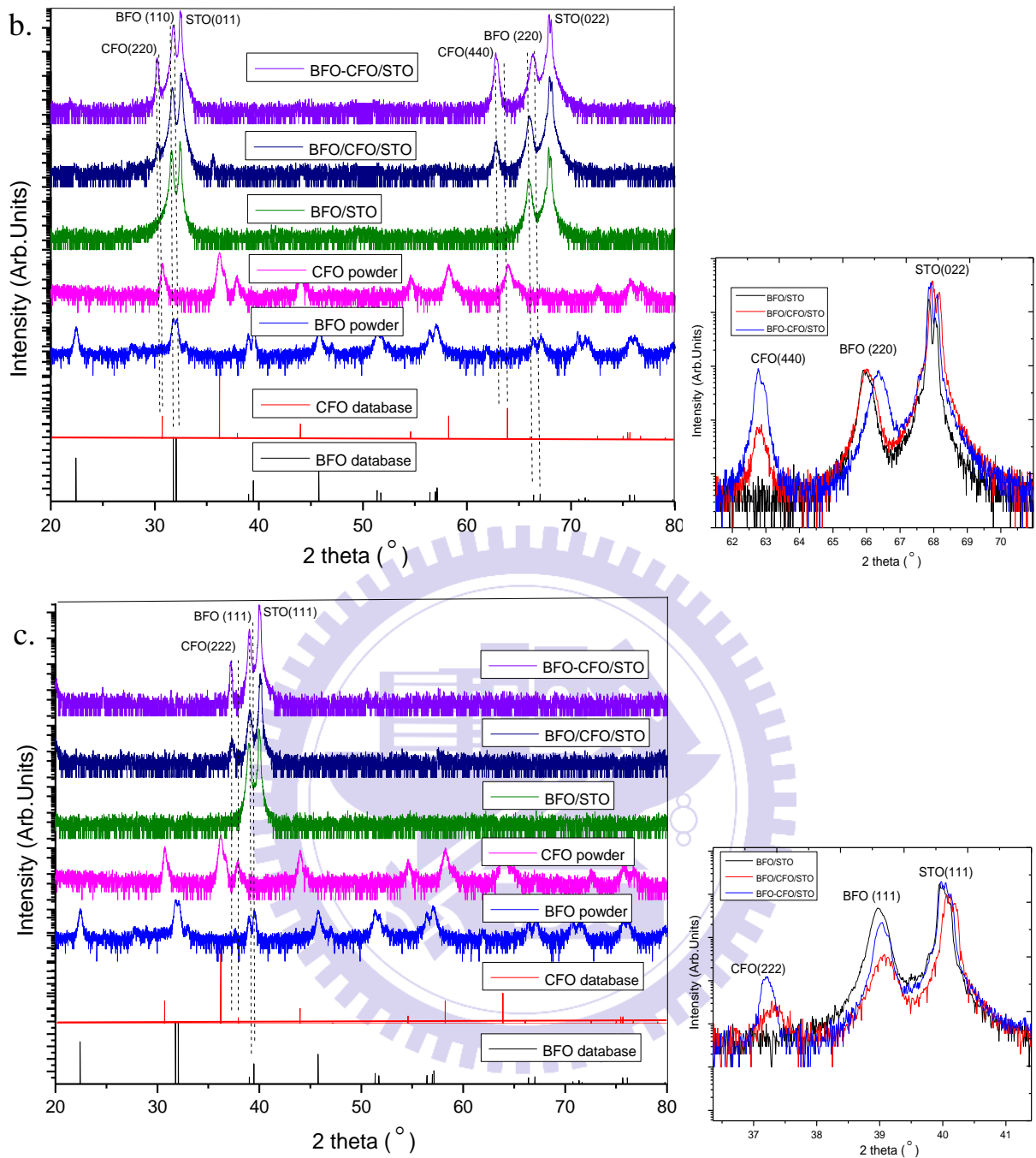from the substrate. Even though the lattice mismatch between BFO and STO is small. By using the Bragg equation, lattice paramaters and strain effects were calculated and summarized in Table 2 and 3.

$$\lambda = 2d_{hkl}\sin\theta_{hkl} \tag{5}$$

$$d_{hkl} = 1.54\text{Å}/2\sin\theta_{hkl} \tag{6}$$

$$d_{hkl} = \frac{a_0}{\sqrt{h^2 + k^2 + l^2}} \tag{7}$$

$$\text{Fix } \lambda \text{ (Cu k}\alpha\text{)} = 1.54\text{Å} \tag{8}$$

Table 2. Strain effect from sample on STO (001).

Sample	Film	Lattice Parameter			Strain		
		010 (Å)	020/040 (Å)	030 (Å)	010 (%)	020 (%)	030 (%)
BFO powder	BFO	3.945	3.961	3.994	-	-	-
CFO powder	CFO	8.395	8.390	8.394	-	-	-
BFO/STO	BFO	4.043	4.054	4.052	2.48	2.34	1.45
BFO/CFO/ STO	BFO	4.044	4.047	4.051	2.51	2.17	1.43
	CFO	-	8.406	-	-	0.92	-
BFO-CFO/STO	BFO	3.966	3.971	3.97	0.53	0.25	0.61
	CFO	-	8.402	-	-	0.14	-

Table 3. Lattice mismatch from sample on STO (001).

Material	Å	Lattice mismatch
STO	3.91	STO-BFO=~1.3%
BFO	3.96	STO-CFO=~7.3%
CFO	8.39	BFO-CFO=~5.9%

Because STO has smaller lattice parameter than that of BFO, leading to a slight in-plane compressive strain on BFO film and a slightly larger lattice

parameter along the out-of plane orientation. As a result, the XRD peak shift to smaller 2θ degree. Shifts of XRD peak in BFO/STO singel layer and BFO/CFO/STO bilayer are larger than that in BFO-CFO/STO VAN. This is indicative that in BFO-CFO/STO VAN there was relaxation effect on BFO film from CFO film in the vertical side. This can be further visualized from the schematic illustration shown in Fig. 27.
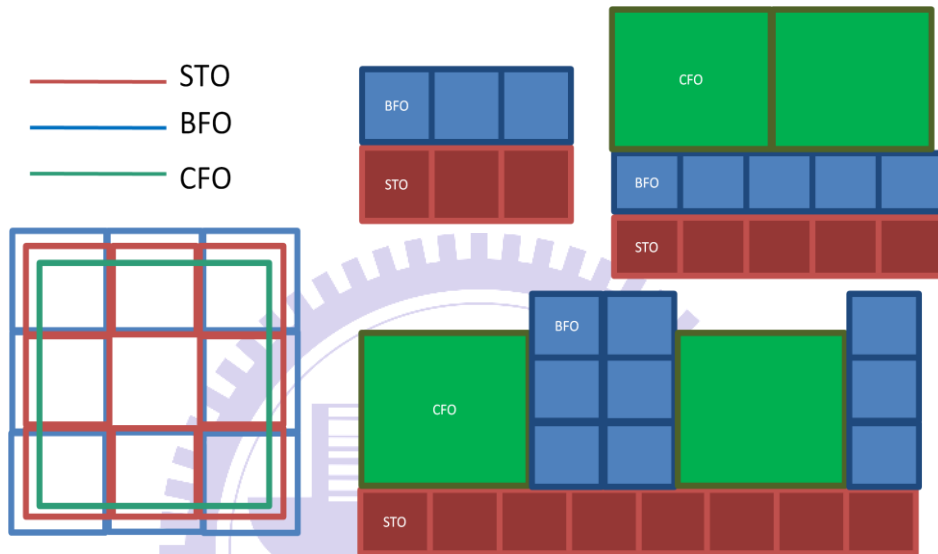
Figure 27. Schematic illustration of strain and relaxation effect in BFO-CFO on STO substrate.(a.) BFO/STO single layer, (b.) BFO/CFO/STO bilayer, (c.) BFO-CFO/STO VAN.

Fig. 28, illustrates the nucleation and growth procedure for individual phases on STO with different orientations, which indicate the expected grain and surface morphologies for films and nanocomposites. Thus from Fig.29 swohs the surface structure analysis obtained by AFM measurements for single layer BFO/STO, bilayer BFO/CFO/STO and BFO-CFO/STO VAN grown on different orientations of STO substrate. From the AFM result, it can be seen that surface of CFO films is rougher that that of BFO film. This might be because CFO has different crystal structure with BFO and STO. The surface morphology of the single layer and bilayer samples appear to vary with the orientation of the STO substrates, which can be explained by the illustrations shown in Fig. 28.
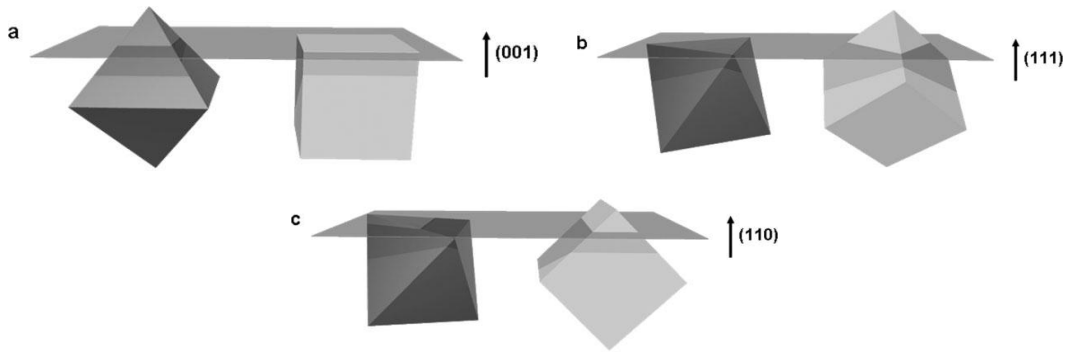
Figure 28. CoFe$_2$O$_4$ (left) and BiFeO$_3$ (right) nucleating on (a.) (001), (b.) (111), and (c.) (110) SrTiO$_3$ surfaces [16].

For BFO-CFO/STO nanocomposite, it is obvious that there are nanopillars embedded in matrix. Depending on the orientation of the STO substrate, the shape of pillars is different. On STO (001), the embedded CFO pillar appears to be rectangular. It becomes like maze pattern on STO (011) and turns into triangular when STO (011) substrate was used. That was happen because as has been discussed in previous chapter, this is due premarily to the different wetting condition on different STO substrates direction.

Figure 29. AFM result : (from left to right) a, b, c. Single layer on STO (001), (011), (111), d, e, f. Bilayer on STO (001), (011), (111) g, h, i. Vertically aligned nanocomposite on STO (001), (011), (111).

To confirm the film surface morphologies, SEM was also used to observe nanopillar of BFO-CFO/STO VAN grown on STO substrates with different direction. As can be seen from the result shown in Fig. 30, essentially same result are observed as those revealed by AFM measurement.

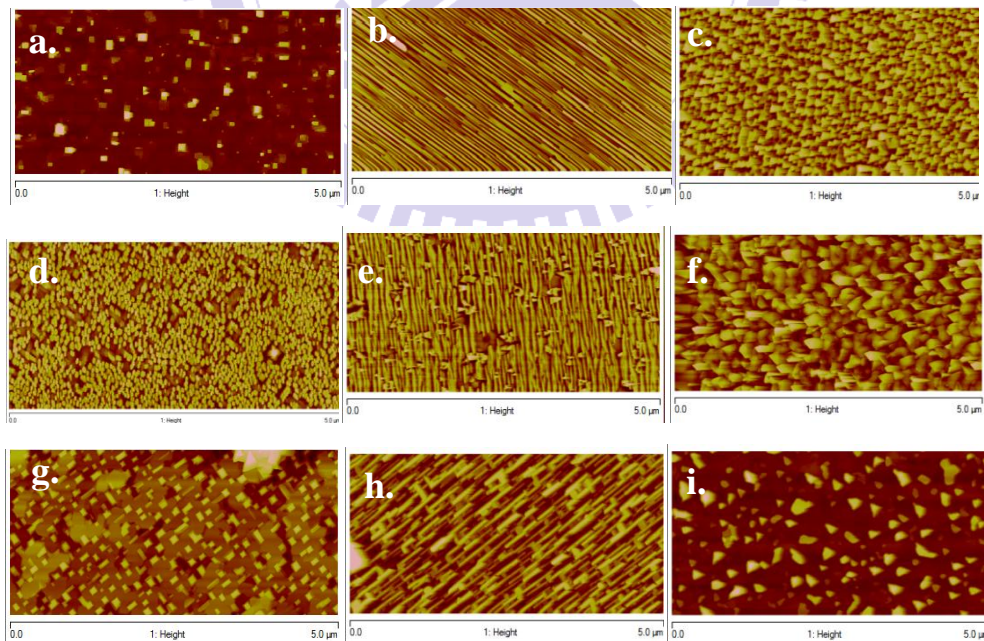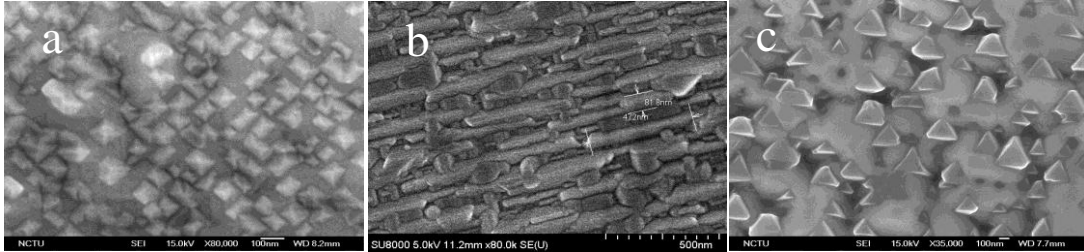Figure 30. SEM result from : BFO-CFO/STO vertical allign nanocomposite. a. (001), b. (011), c. (111).

One of primary goals of this reseach is also try to manipulate pillar density in the sample and hence the coupling between the two phases. Fig. 31 demonstrate that this can be done by varying the respective deposition time of BFO and CFO in each cycles.
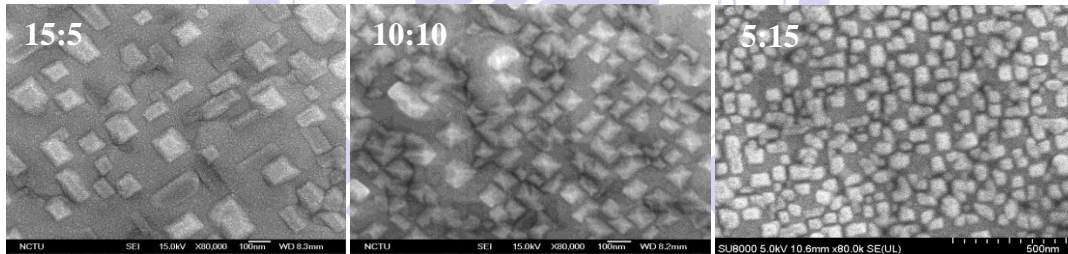
Figure 31. SEM result from BFO-CFO/STO (001) vertical allign nanocomposite with variation of CFO pillar density.

The left photograph in Fig. 31 has the lowest pillar density because the deposition time are 15 second for BFO and 5 second for CFO respectively, with a total deposition time of 30 minutes, each target has experienced 180 cycles during the process. In the middle photograph, both BFO and CFO targets was deposited by using a 10/10 second cycle. Finally the right photograph is obtained by using 5 second deposition time for BFO and 15 second for CFO.

Since on STO (001) substrate, CFO is the pillar, so if we want to reach higher pillar density, deposition time of CFO should be higher than BFO and vice versa.

4.2 Properties Analisys

As mentioned previously, the Raman measurement showed clear phase transitions at ~140 K and ~200 K, although the exact origin of which is as yet unclear, it has been tentatively attributed to spin reorientations [20]. Thus, this study has focused more on the magnetic and electric properties at lower temperatures in particular, combination BFO and CFO is expected to result in extra coupling between them and the anomaly occured in BFO at low room temperature may be further modified.

Figure 32. M-T measurement for BFO/STO single layer on STO a. (001), b. (011), c. (111), d. From refrences [8] BFO single crystal powder.
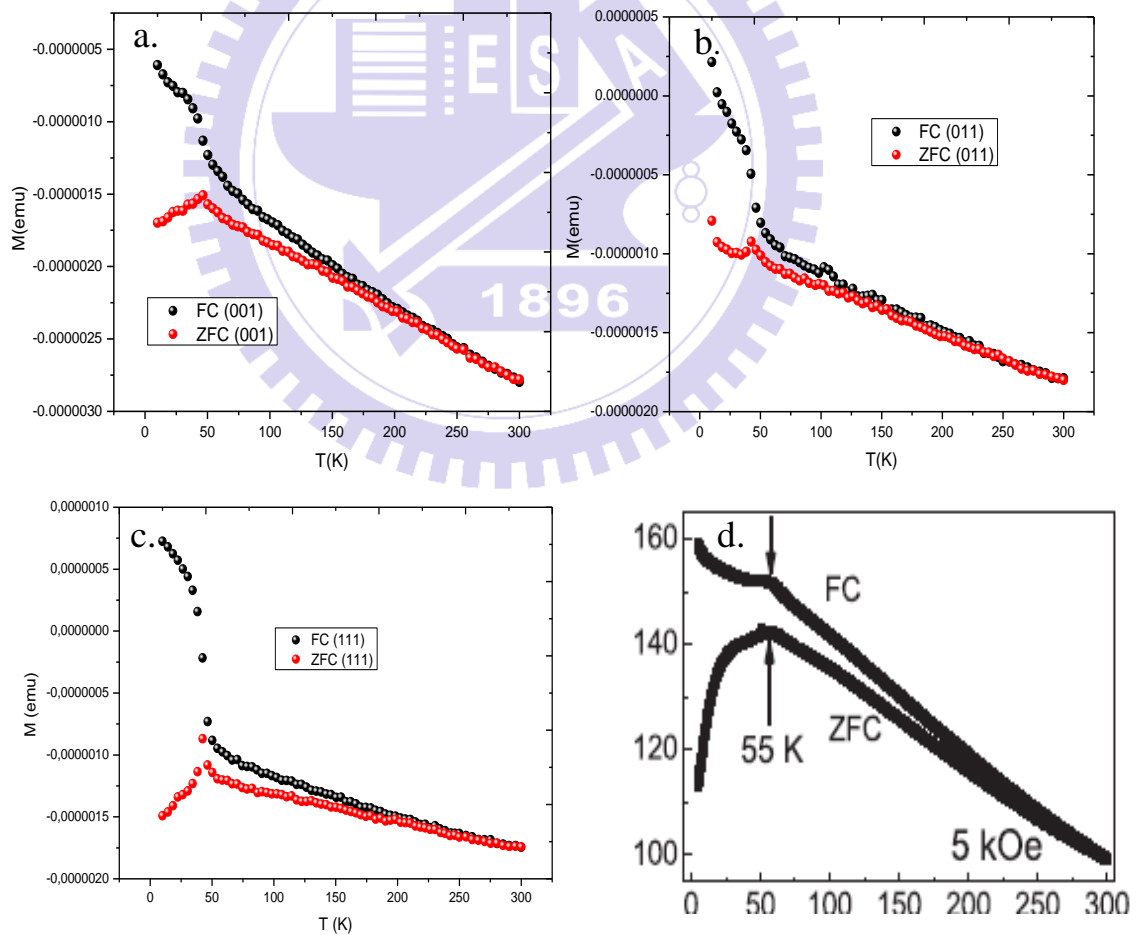
41

Fig. 32 shows the temperature-dependent magnetization (M-T) obtained for single layer BFO film grown on various STO substrates. Similar to that observed in BFO single crystal powder (Fig. 32 d) the M-T beharviours of BFO/STO single layer are having two magnetic phase transitions. Nevertheles, the temperetures are systematically lower in films as compared to that in single crystals. For films, the FC and ZFC curves start to split around 160 K for all BFO/STO (001), (011), and (111). Whereas for BFO single crystal it have been reported in [29-34] that there were four anomalies occuring at 50 K, 140 K, 200 K, and 230 K, respectively. It has been further identified that the 50 K transition is magnetic, but glassy and with magnetoelectric coupling, whereas the140 K, 200 K, and 230 K transition were dominantly magnetic, magnetoelastic with small coupling to polarization, and glassy, respectively [35].

In the present BFO/STO single layer, the transition at 30 K and 160 K might be associated to the 50 K and 200 K transitions described above. Consequently, it is suggestive that the magnetoelectric coupling is still playing a substantial role in these BFO/STO single layer. It is noted that there is negative magnetization in all M-T curve, this is belived to arise from the diamagnetic nature of STO substrates. Furthermore the lowering of transition temperatures may be due to the strain effect, making the magnetoelectric coupling being slightly modified.
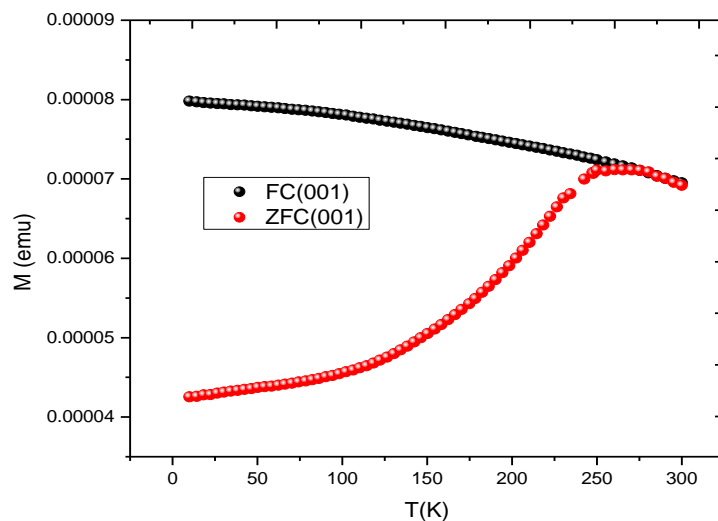

Figure 33. M-T measurement for CFO/STO (001) single layer.

M-T measurement for CFO/STO single layer shown in Figure 33, also related to CFO nanoparticle M-T measurement shown in Fig. 16 before. There is increasing FC curve from 300 K to 12 K, which mean there was large magnetization at 300 K suggested the system is in ferromagnetic state. Than also in ZFC curve found temperature blocking (T_B) around 250 K which also little shift to higher temperature compare than CFO nanoparticle which occur around 240 K, because it might be affect of strain effect from STO substrate to CFO film. Thus, compare than BFO/STO single layer, diamagnetic affect in CFO/STO single layer from STO substrate was dissapear because magnetic in CFO is stronger than BFO.
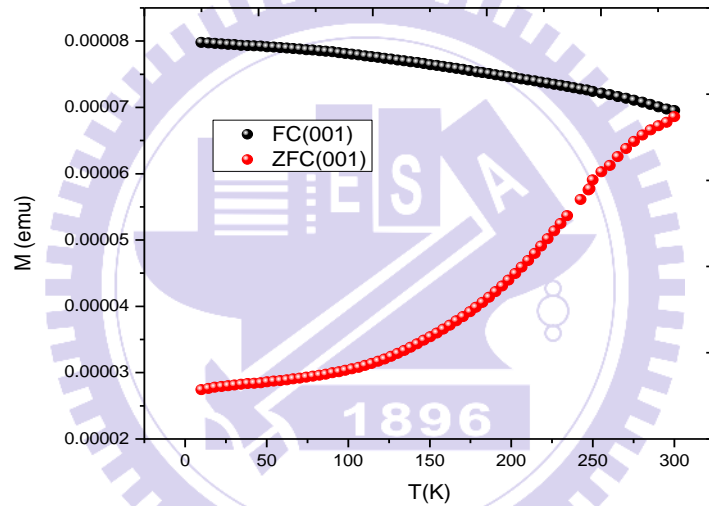
Figure 34. M-T measurement for BFO/CFO/STO (001) bilayer.

This reseach tried to observe some magnetoelectric properties below room temperature when BFO is combined by CFO. Fig. 34 shows the M-T beharvior of BFO/CFO bilayer films. The result, to our surprise, are quite different from that of single layer BFO/STO single layer (Fig. 32). There is no obvious magnetic phase transition like BFO/STO single layer. The FC and ZFC curves start to split around 300 K. The anomaly around 30 K also cannot be observed anymore. This indicates that the ferromagnetic CFO may have suppressed magnetoelectric coupling for BFO alone. Magnetic anomaly which occurs in BFO because of spin magnetic reorientation, it disapears because the spin

magneitc reorientation is suppressed by spin locking originated from ferromagnetic CFO. The large magnetization at 300 K also suggest the whole system is in ferromagnetic state due to existance of CFO, which those beharvior also same with FC curve in M-T measurement for CFO/STO single layer sample. For ZFC, it was also like belong in CFO/STO single layer beharvior, but in this case might be 300 K is the T_B, which T_B in BFO/CFO on STO bilayer was shift to the higher temperature at 300 K compare than CFO nanoparticle which occur in 240 K (Fig. 16) and CFO/STO single layer which occur in 250 K (Fig. 33), because there was coupling between antiferromagnetic-ferromagnetic which might be change energy barriers of the magnetic anisotropy in CFO. The measurement also shows that magnetization stay at positive value, because the ferromagnetic effect from CFO which reduces diamagnetic behavior from STO substrate.

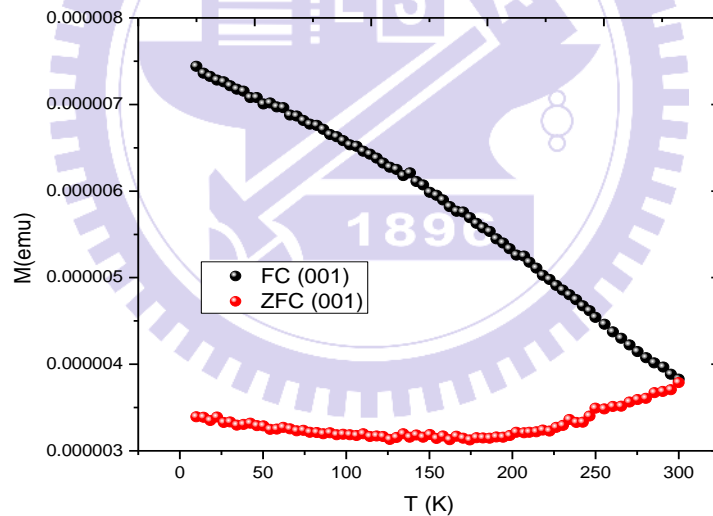Figure 35. M-T measurement for BFO-CFO/STO (001) VAN.

Fig. 35 shows the M-T beharvior for BFO-CFO/STO (001) VAN. The beharvior is similar to that of BFO/CFO/STO (001) bilayer, with the FC and ZFC curves being split at room-temperature. However, the FC appear to show progressive magnetization as the temperature is lowered, suggesting that the magnetization state of this BFO-CFO/STO VAN system is somewhat different

from that of the bilayer system. Since the external field was applied in-plane, it might pick up more contribution from the BFO phase in the VAN system than in bilayer system. Nevertheles, more investigation are certainly needed to unveil and understand the features. In any case, both result did suggest some possible magnetic coupling between BFO and CFO, which in turn modifies the spin. Reorientation associated magnetization anomalies described before.
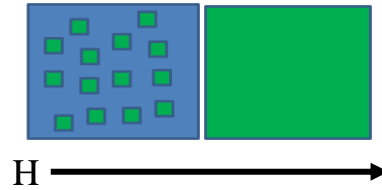

Figure 36. BFO-CFO/STO VAN (left) BFO/CFO/STO bilayer (right). CFO distribution in BFO-CFO/STO VAN is discontinue. Magnetic field applied parallel to the sample.

For electric properties, capacitance measurement and resistance measurement were caried out to observe the dielectric and transport properties of the samples. Recently detailed investigation of the bulk magnetic, dielectric and thermal properties of high quality single crystals of BFO in the wide temperature range of 1.5–800 K has been reported [27, 28]. The results were not consistent with numerous phase transitions below the Néel temperature reported in references [29-34]. Especially, temperature dependences of the dielectric constant and heat capacity show absence of any phase transition below room temperature. Magnetic study reveals no evidence low-temperature ($T < T_N$) magnetic phase transitions as well as spin-glass behavior [35].

Capacitance measurement set up used to measure capacitance from the sample is shown in Fig. 36. NSTO (STO doped Nb) substrate was used as the bottom electrod and the top electrode was silver paste or In. The obtained result for various samples are shown in Fig. 38-40.
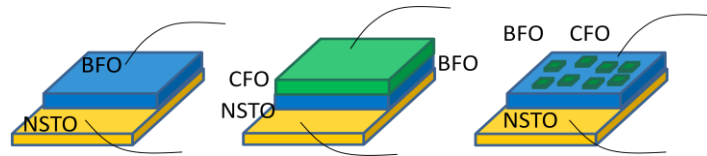
Figure 37. Capacitance measurement set up.

Generally, the capacitance of all samples (single layer, bilayer, and vertically allign nanocomposite) decreases with decreasing temperature. This indicates that the dielectric constant decrease with decreasing temperature, as well. Since the dielectric constant is related to the ease of dipole movement and hence polarization, the result seems to suggest that the dipoles are easier to move or the polarization is diminishing at lower temperatures. Moreover, the capacitance also decreases with increasing frequency that used. Lower frequency could detect all possibile polarizations which occur in the sample like electronic polarization, ionic polarization, and dipole polarization directly (see Fig. 11). Therefore, it is reasonable to obtain higher capacitance at lower measuring frequencies.

In order to understand these general beharviours, more detailed comparisons among different sample are in order. Fig. 38 shows the capacitance measurement from the BFO/NSTO single layer. The result clearly show sign of anomaly around 30 K and 200 K, which are slightly lower than 55 K and 215 K for BFO bulk. As mentioned before, it might be due to the strain effect from NSTO substrate to BFO film. Dielectric and conductivity anomalies have been reported [21] to occur at T_N=643 K (370 ^{o}C), and was attributed to magnetoelectric coupling during the phase transition. The magnetodielectric coupling is also responsible for the reported anomaly in the birefringence of BFO at T_N [22]. The questions is what is responsible for the anomalies observed at temperatures below room-temperature.
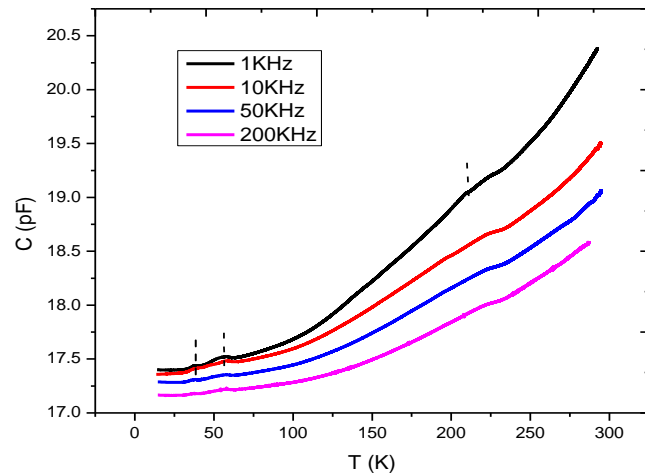
Figure 38. Capacitance vs temperature measurement from BFO/NSTO single layer.

It is clear that capacitance has istimate relation with dielectric. Thus capacitance anomalies around 30 K, 50 K and 200 K observed in this BFO/NSTO (001) single layer (Fig. 38) should have similar origin as those identified in BFO single crystals [4], where the dielectric anomaly has been attributed to the magnetic (or magnetoelastic) transitions. The anomalies do not seem to affect the dielectric loss (tan δ). As reported in previous M-T measurements, there are similar magnetization anomalies around 30 K and 160 K for the single layer BFO, which is consistent with the conjectures derived from the single crystal [4].

Figure 39. Capacitance vs temperature measurement for BFO/CFO bilayer on NSTO (001) substrate.

As shown in Fig. 39, for the BFO/CFO on NSTO (001) bilayer, there was no describe capacitance anomaly can be observed. Since the capacitance anomaly is belived to arise from the magnetic (or magnetoela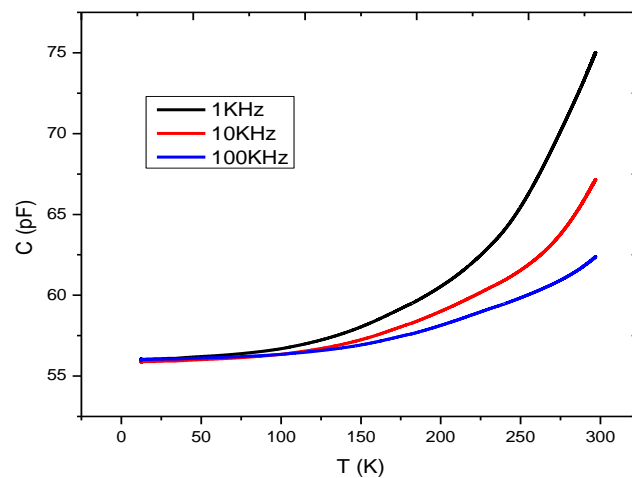stic) transitions associated with magnetic reorientation [4], the absence of anomaly in the bilayer system might imply the hindrance of such magnetic reorientations. The fact that both M-T and C-T measurement displays the same feature, i.e. no low temperature anomalies, strongly suggest that the spin reorientation activities are quenched by coupling to the ferromagnetic CFO phase. Nevertheles, further experiments are certainly needed to deliriate the real underlying mechanism.
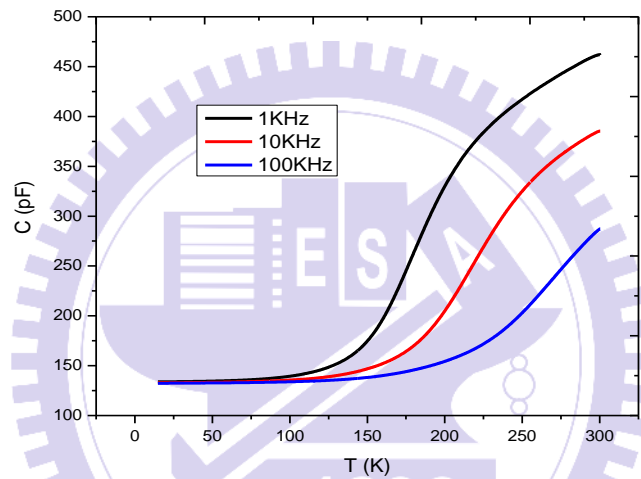
Figure 40. Capacitance vs temperature measurement for BFO-CFO VAN on NSTO (001) substrate.

Finally for, BFO-CFO vertically allign nanocomposite on NSTO (001), although the capacitance measurement also shows similar temperature and frequency dependences as that seen in single layer and bilayer system, there is some distinct feature in this case. As been clearly seen in Fig. 38, the C-T curves shows two distinct slope changes as the temperature is decreased from room-temperature to low temperature. Since in this structure CFO pillars are embedded in BFO matrix, the magnetic coupling-induced effect of the polarization in the BFO is expected to be more complicated and ubiquitous. It is noted that due to the much relaxed strain in films the temperatures at which the

slope change in C-T curves occured are much higher than that observed in single and bilayer system.

The interpretation to the observed M-T and C-T result of composite system in terms of magnetoelectric properties apparently are much more difficult to comprehend. The usual anomalies seems in the single crystal and single layer samples are again absence as that exhibited in BFO/CFO bilayer system. This is suggestive that the magnetoelectric transitions associated with spin rearientation in BFO phase has been similarly suppressed by the existence of CFO pillars. But the slope changes seem at 140 K and 230 K require further explanations which, unfortunatelly, are not avaible at present. Nevertheles, it is noted that since the temperatures are very close to the dielectric anomalies seem in single crystal sample, it may reflect the changes in BFO matrix. However, the incorporation of CFO pillars may change the over all capacitance (i.e. parallel capacitors with different dielectrics in between), which in term gives rise to the specific features of slope changes seem in this composite system. We are looking into this by examining the beharvior exhibited by samples with different CFO pillars density.
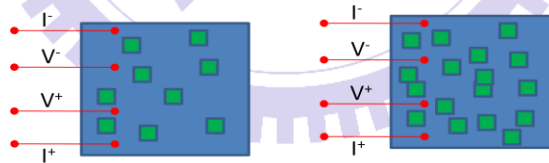
Figure 41. R-T measurement set up for BFO-CFO VAN on STO (001) with different CFO pillar density.

Fig. 42 compares the R-T beharviors of single layer BFO, low pillar density BFO-CFO VAN, and high pillar density BFO-CFO VAN samples. The measurement set up are depicted in Fig. 41. From the result displayed in Fig. 42, it is evident that the film with higher density of embedded CFO pillars turns from insulating beharvior into metallic near T ≈ 30 K. Since in these temperatures BFO presents as the continous matrix phase, it is evident that the

49

proximity of ferromagnetic CFO phase has eventually introducing significant effect to the BFO phase.

Figure 42. R-T measurement in BFO/STO (001) single layer and BFO-CFO/STO (001) VAN with different CFO pillar density.

As has been demonstrated previously [25], the electric transport property of BFO is primarily governed by thermally activated process at high temperature and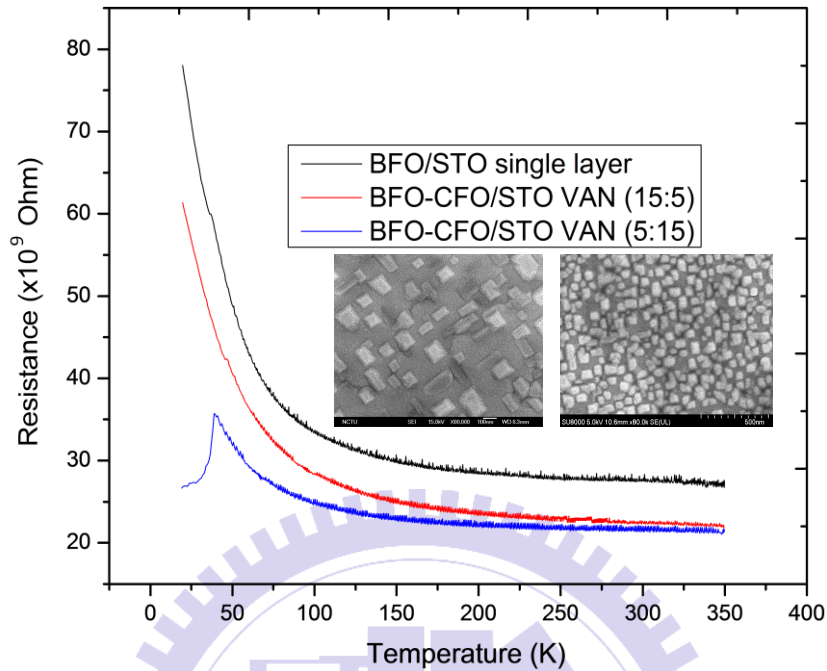 turned into Variable Range Hopping (VRH) – dominant process at lower room temperatures. It was further indicated that the VRH-dominant transport process is further dominated by ferroelectric domain walls in BFO phase. Thus by applying a strong enough magnetic field, it is possible to turn the material into metallic and obtain substantial magnetoresistance ratio.

In our case here, although neither the single layer BFO film nor the low - pillar density composite film shows the signature of thermally-activated to VRH transport transition, the insulator-like to metal-like transition seen in the high-pillar density sample does imply the substantial effect of ferromagnetic coupling to the transport properties of the BFO matrix. It should be interisting to conduct more experiments to set out these emergent phenomena.

50

V. Conclusion

From the data and the discussions presented in preciding chapters some tentative conclusions are reached as following:

- BFO-CFO vertically align nanocomposite was succesfully made by utilizing the different wetting conditions from BFO and CFO film when growing on STO substrate at the same time in the PLD system.

- There was strain effect from STO substrate to BFO and CFO film. Especially for BFO-CFO/STO VAN, CFO pillar give vertical relaxation to the strain of BFO film.

- Because of strain effect from STO substrate to BFO film, there was shifting of magnetic phase transitions on BFO/STO thin film around 30 K and 160 K comparedto that of BFO powders where the transition occur around 55 K and 200 K, respectively.

- From M-T and C-T measurement from BFO/CFO bilayer and BFO-CFO VAN, antiferromagnetic-ferromagnetic coupling (BFO-CFO) is stronger than antiferromagnetic-ferroelectric coupling (BFO). Making the magnetization and capacitance anomalies unobservables in those system.

- The C-T beharviors of BFO/NSTO and BFO/CFO/NSTO are in general similar, but different in subtle details, which presumably originates from the quenching of spin reorientation in BFO due to ferromagnetic coupling from CFO. The situation is even more complicated in the CFO pillar embedded in BFO matrix sample.

- The high-density BFO-CFO/STO VAN film showed an apparent insulator-metal transition around 30 K, which is similar to that observed in BFO film under strong external magnetic fields [25]. The result suggest that when the pillar density is large enough it may generate strong enough local magnetic field to modify the ferroelectric domain

structures in BFO matrix.

- Further investigations are certainly in order to delineate the interisting emergent phenomena observed in the present study.

Bibliographies

[1] L. W. Martin, Y. H. Chu, R. Ramesh, "Advances in the growth and characterization of magnetic, ferroelectric, andmultiferroic oxide thin films", Materials Science and Engineering, R 68, 89–13, 2010.

[2] D. G. Schlom, J. H. Haeni, J. Lettieri, C. D. Theis, W. Tian, J. C. Jiang, X. Q. Pan, Mater. Sci. Eng. B 87, 282, 2001.

[3] J. Van den Boomgaard, D. R. Terrell, R. A. J. Born, J. Mater. Sci. 9, 1705, 1974.

[4] S. A. T. Redfern, C. Wang, J. W. Hong, G. Catalan, J. F. Scott, J. Phys.: Cond. Mat., 20, 452205, 2008.

[5] J J.F. Scott, C.A. Paz de Araujo, Science, 246, 1400, 1989.

[6] F. Jona, G. Shirane, Ferroelectric Crystals, Dover Publications, New York, 1993.

[7] J. Ray et al., Journal of Magnetism and Magnetic Materials 324, 4084–4089, 2012.

[8] Fiebig, J. Phys. D. 38, R123, 2005.

[9] Princeton University, Solid State Chemistry Research Group, Page of Cava Lab.

[10] Haimei Zheng, Qian Zhan, Florin Zavaliche, Matt Sherburne, Florian Straub, Maria P. Cruz, Long-Qing Chen, Uli Dahmen, and R. Ramesh, "Controlling Self-Assembled Perovskite-Spinel Nanostructures", Nano Letter, Vol. 6, No. 7, 1401-1407, 2006.

[11] M. Ohring, Materials Science of Thin Films: Deposition and Structure, Academic Press, San Francisco, 2002.

[12] Jing Ma, Jiamian Hu, Zheng Li, and Ce-Wen Nan, Adv. Mater. XX, 1–26, 201003636, 2011.

[13] N. Dix , R. Muralidharan, J. M. Caicedo, D. Hrabovsky, I. Fina, L. Fa`brega, V. Skumryev, M.Varela, J. Guyonnet, P. Paruch, F. Sa´nchez, J. Fontcuberta. Journal of Magnetism and Magnetic Materials 321, 1790–1794, 2009.

[14] H. Bea, M. Bibes, A. Barthelemy, K. Bouzehouane, E. Jacquet, A. Khodan, J. P. Contour, S. Fusil, F. Wyczisk, A. Forget, D. Lebeugle, D. Colson, M. Viret, Appl. Phys. Lett. 87, 072508, 2005.

[15] R. Muralidharan, N. Dix, V. Skumryev, M. Varela, F. Sánchez, and J. Fontcuberta. App. Phy, 103, 07E301, 2008.

[16] Haimei Zheng, Florian Straub, Qian Zhan, Pei-Ling Yang, Wen-Kuo Hsieh, Florin Zavaliche, Ying-Hao Chu, Uli Dahmen, and Ramamoorthy Ramesh, "Self-Assembled Growth of BiFeO$_3$–CoFe$_2$O$_4$ Nanostructures", Adv. Mater, 18, 2747–2752, 2006.

[17] W. Eerenstein, N. D. Mathur, J. F. Scott, Nature 442, 759, 2006.

[18] J. Nogue´s, I. K. Schuller, J. Magn. Magn. Mater. 192, 203, 1999.

[19] The University of Southern Mississippi, School of Polymers and High Performance Materials, Page of the research group of Dr. Kenneth A. Mauritz.

[20] Gustau Catalan, James F. Scott, "Physics and Applications of Bismuth Ferrite", Adv. Mater., 21, 2463–2485, 2009.

[21] M. Polomska, W. Kaczmarek, Z. Pajak, Phys. Stat. Sol., 23, 567, 1974.

[22] J. F. Scott, JETP Lett. 1989, 49, 233, 100, 033908, 2006.

[23] R. Mazumder, S. Ghosh, P. Mondal, D. Bhattacharya, S. Dasgupta, N. Das, A. Sen, A. K. Tyagi, M. Sivakumar, T. Takami, H. Ikuta, J. Appl. Phys.

[24] G. Catalan, Appl. Phys. Lett., 88, 102902, 2006.

[25] He Q., Yeh C. H., Yang J. C., Singh-Bhalla G., Liang C. W., Chiu P.W., Phys. Rev. Lett., 108:067203, 2012.

[26] Xing-Hua Li, Cai-Ling Xu, Xiang-Hua Han, Liang Qiao, Tao Wang, Fa Shen Li, Nanoscale Res. Lett., 5:1039–1044DOI 10.1007/s11671-010-9599-9, 2010.

[27] T. Hyeon, Y. Chung, J. Park, S. S. Lee, Y. W. Kim, B. H. Park, J. Phys. Chem. B 106, 6831, 2002.

[28] Jill Guyonnet,"Studies of Magnetoelectric Coupling in $BiFeO_3$-$CoFe_2O_4$ Nanocomposite", Universit´e de Gen`eve Facult´e des SciencesD´epartement de Physique de la Mati`ere Condens´ee, Master, 2008.

[29] M. K. Singh, W. Prellier, M. P. Singh, R. S. Katiyar, J. F.Scott, Phys. Rev. B ,77, 144403, 2008.

[30] M. K. Singh, R. S. Katiyar, W. Prellier, J. F. Scott, J. Phys.:Condens. Matter , 21, 042202, 2009.

[31] M. K. Singh, R. S. Katiyar, J. F. Scott, J. Phys.: Condens.Matter, 20, 25203, 2008.

[32] M. Cazayous, Y. Gallais, A. Sacuto, R. de Sousa, D. Lebeugle, D. Colson, Phys. Rev. Lett., 101, 37601, 2008.

[33] S. A. T. Redfern, Can Wang, J. W. Hong, G. Catalan, J. F. Scott, J. Phys.: Condens. Matter , 20, 452205, 2008.

[34] G. Catalan, J. F. Scott, Adv. Mater., 21, 2463, 2009.

[35] E. P. Smirnova, A. Sotnikov, S. Ktitorov, N. Zaitseva, H. Schmidt, M. Weihnacht, Eur. Phys. J. B, 83, 39–45, 2011.

[36] J. Lu, M. Schmidt, P. Lunkenheimer, A. Pimenov, A. A. Mukhin, V. D. Travkin, A. Loidl, J. Phys. Conf. Ser., 200,012106, 2010.

[37] J. Lu, A. G. unther, F. Schrettie, F. Mayr, S. Krohns, P. Lunkenheimer, A. Pimenov, V. D. Travkin, A. A. Mukhin, A. Loidl, Eur. Phys. J. B, 75, 451, 2010.

Autobiography

Personal Details

Full Name : **Tahta Amrillah**

Sex : male

Place, Date of Birth : Pamekasan-Indonesia, November 29, 1989

E-mail : tahvisikawan@gmail.com

Educational Background

2008-2012 : Material Science in Physics Department, Sepuluh Nopember Institute of Teknologi - ITS, Surabaya-Indonesia, B. S. Degree in Physics

2012-2014 : Electrophysics Department, National Chiao Tung University - NCTU, Hsinchu-Taiwan, M. S. Degree in Electrophysics.